JCI insight

Murine CAR19 Tregs suppress acute graft-versus-host disease and maintain graft-versus-tumor responses

Sara Bolivar-Wagers, … , Christopher A. Pennell, Bruce R. Blazar.

JCI Insight. 2022. https://doi.org/10.1172/jci.insight.160674.

Research In-Press Preview Immunology Transplantation

Graphical abstract

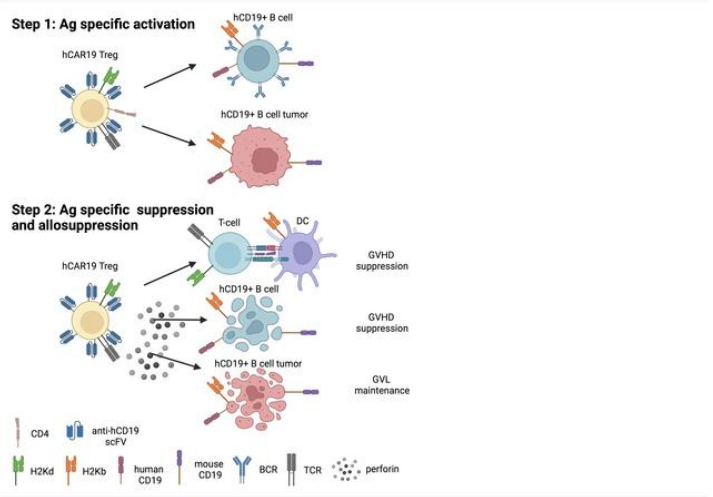

Murine CAR19 Tregs suppress acute graft-versus-host disease and maintain graft-versus-tumor responses

Sara Bolivar-Wagers[1], Michael L. Loschi[1], Sujeong Jin[1], Govindarajan Thangavelu[1], Jemma H. Larson[1], Cameron S. McDonald-Hyman[2], Ethan A. Aguilar[1], Asim Saha[1], Brent H Koehn[1], Mehrdad Hefazi[3], Mark J. Osborn[1], Michael C. Jensen[4], John E. Wagner[1], Christopher A. Pennell[5], Bruce R. Blazar[1].

[1]Department of Pediatrics, Division of Blood & Marrow Transplant & Cellular Therapy, University of Minnesota, Minneapolis, Minnesota, USA. [2] Department of Medicine, Division of Hematology/Oncology/Transplantation, University of Minnesota, Minneapolis, Minnesota, USA. [3]Department of Internal Medicine, Division of Hematology, Mayo Clinic, Rochester, Minnesota, USA. [4]Department of Pediatrics, Division of Hematology and Oncology, University of Washington, Seattle, Washington, USA. [5]Department of Laboratory Medicine and Pathology, University of Minnesota, Minneapolis, Minnesota, USA.

Authorship note: SBW and MLL are co–first authors.

Conflict of interest: BRB has received remuneration as an advisor to Magenta Therapeutics and BlueRock Therapeutics; research funding from BlueRock Therapeutics, Rheos Medicines, Carisma Therapeutics, Inc., and is a co-founder of Tmunity Therapeutics.

Address correspondence: Bruce R. Blazar, MMC 366 Mayo, University of Minnesota, 420 Delaware St SE, Minneapolis, Minnesota 55455, USA. Phone: 612.626.2961; Email: blaza001@umn.edu.

Key Words: GVHD, GVL, Regulatory T-cells, CAR Tregs, CAR T-cells

Abstract

Allogeneic hematopoietic stem cell transplantation (allo-HSCT) efficacy is complicated by graft-versus-host disease (GVHD), a leading cause of morbidity and mortality. Regulatory T-cells (Tregs) have shown efficacy in preventing GVHD. However, high Treg doses are often required, necessitating substantial *ex vivo* or *in vivo* expansion that may diminish suppressor function. To enhance *in vivo* suppressor function, murine Treg were transduced to express an anti-human CD19scFv chimeric antigen receptor (hCAR19) and infused into lethally irradiated hCD19 transgenic recipients for allo-HSCT. Compared to recipients receiving control transduced Tregs, those receiving hCAR19 Tregs had a significant decrease in acute GVHD lethality. Recipient hCD19 B-cells and murine hCD19TBL12^{luc} lymphoma cells were both cleared by allogeneic hCAR19 Tregs indicative of graft-versus tumor (GVT) maintenance and potentiation. Mechanistically, hCAR19 Tregs killed syngeneic hCD19+ but not hCD19- murine TBL12^{luc} cells *in vitro* in a perforin-dependent, granzyme B-independent manner. Importantly, cyclophosphamide treated hCD19 transgenic mice given hCAR19 cytotoxic T-lymphocytes without allo-HSCT experienced rapid lethality due to systemic toxicity that has been associated with proinflammatory cytokine release; in contrast, hCAR19 Treg suppressor function enabled avoidance of this severe complication. In conclusion, hCAR19 Tregs are a novel and effective strategy to suppress GVHD without loss of GVT responses.

Introduction

Allogeneic hematopoietic stem cell transplantation (allo-HSCT) can be a curative therapy for hematological malignancies (1, 2). However, a leading consequence of allo-HSCT is graft-versus-host disease (GVHD), an immune-mediated multi-organ inflammatory disease and a leading cause of morbidity and mortality after allo-HSCT (3). Despite current GVHD prophylactic regimens, 30-70% of allo-HSCT patients still develop GVHD leaving patients more susceptible to infection and relapse (3-8). Pre-clinical and clinical studies show that adoptive transfer of regulatory T-cells (Tregs) can be highly effective at preventing GVHD (9-16). However, clinical translation has been hampered by the requirement for high Treg cell doses and variability in Treg potency to achieve therapeutic effects.

On a per cell basis, antigen-specific Tregs are superior to polyclonal Tregs as suppressors of cognate antigen responses. By restricting antigen specificity, the risk for systemic immune suppression may be diminished and the effective cell dose reduced (17). Chimeric antigen receptors (CARs) can redirect Tregs to a desired antigen (18). For example, anti-HLA-A2 specific CAR Tregs suppress HLA-A2 disparate solid organ graft rejection (17). While this approach targets one of the most common HLA class I allelic mismatched antigens, HLA-A2 is present in only 34.6% of African Americans (19). Thus, there is a need to redirect Tregs towards more readily available target antigens. CAR T-cells also are being investigated for the treatment of autoimmunity. For example, CD19 directed CAR (CAR19) T-cells can effectively treat murine systemic lupus erythematous by killing B-cells (20) and T-cells expressing chimeric autoantigen receptors (CAARs) can engage in targeted killing of autoreactive B-cells (21).

Tregs use a variety of pathways to mediate suppression including directed cytolytic activity (22-29). Murine Tregs can regulate immune responses via killing of antigen presenting B-cells in a granzyme B (GzB) dependent, partially perforin dependent manner (23). Additionally, human

Treg redirected through bispecific T-cell engagers (BiTEs) maintained suppression while killing antigen expressing tumor cells in a perforin dependent, partially GzB dependent manner (30). Whereas MacDonald *et al* (2016) reported human HLA-A2 specific CAR Treg killing of HLA-A2+ targets in vitro (17), to date only Boroughs *et al* (2019) has reported in vitro and in vivo killing by human CAR19 Tregs (31). This group demonstrated that human CAR19 Tregs killed CD19+ targets in vitro via the perforin-granzyme pathway, with measurable but low killing of antigen-expressing targets in vivo using a skin allograft model (31). CAR Tregs could theoretically engage in targeted killing while simultaneously performing immunosuppression.

Activation of conventional CAR19 T-cells by CD19+ targets triggers the release of proinflammatory cytokines (e.g., TNFα, IFNγ) which, in turn, induce endogenous myeloid and endothelial cells to secrete additional proinflammatory cytokines (e.g., IL-1ß, IL-6). These amplifying waves of inflammation cause toxicities such as cytokine release syndrome (CRS), an acute systemic inflammatory response with fever and multi-organ dysfunction, and an immune effector cell-associated neurotoxicity syndrome (ICANS) (32-34). Because CAR19 Tregs can kill CD19+ targets directly, we reasoned CAR19 Tregs would have anti-tumor efficacy in vivo. Because Tregs also blunt immune activation of bystander cells, we hypothesized that CAR19 Tregs would be superior to conventional CAR19 T-cells by reducing toxicities caused by systemic inflammation. To test our hypothesis, we developed a mouse model that replicated allo-HSCT for CD19+ B-cell malignancies.

We employed CAR technology to redirect murine Tregs towards human CD19 (hCD19) expressing B-cells. B cells are an ideal target in allo-HSCT models based on their tissue distribution, capacity for antigen presentation and activation of alloreactive T-cells (35), as well as expression on leukemias and lymphomas. We used a murine syngeneic model in which the hCD19 transgene is expressed at hemizygous levels in recipient murine B-cells. We employed

hemizygotes because homozygous hCD19 expression reduces absolute B-cell numbers, and hence the overall number of hCD19 B-cells and the mean hCD19 density on B-cells exceeded that of B-cell lymphoid malignancies as well as non-malignant B-cells (36). Here, we investigated the potential of murine anti-hCD19 CAR (hCAR19) Treg to deplete recipient hCD19+ B cells in vivo and induce systemic toxicity compared to CAR19 T-cells. We then evaluated whether hCAR19 Treg could eliminate murine B-cell lymphoma cells expressing hCD19 (hCD19+ TBL12) cells in vivo without toxicity. Lastly, we tested the potential of hCAR19 Treg to suppress acute GVHD (aGVHD) without abrogating the graft-versus-tumor (GVT) response in a murine major histocompatibility complex (MHC) mismatch allo-HSCT model.

Results

***Generation of hCAR19 Tregs using retroviral vectors*.** Tregs were first enriched from wildtype (WT) or Foxp3-GFP^{+} mice by magnetic-activated cell sorting (MACS) and then flow sorted for CD4^{+}CD25^{hi} or CD4^{+}CD25^{hi}GFP^{+} cells (Supplementary Figure 1). Tregs were activated for three days with anti-CD3/CD28 Dynabeads and human IL-2 prior to retroviral transduction (Figure 1A). hCAR19 Tregs were generated using an pMP71 retroviral vector encoding a single chain variable fragment (scFv) derived from a hCD19 specific monoclonal antibody, FMC63, human CD8α hinge and transmembrane domains, human 4-1BB (CD137) costimulatory domain, and CD3ζ signaling domain (Figure 1B). The plasmid vector contains a viral T2A self-cleaving peptide that permits ribosomal skipping and expression of a functionally inert truncated human epidermal growth factor receptor (tEGFR) (Figure 1B). Tregs were transduced with retroviruses containing or lacking the hCAR19 construct; both constructs encoded the tEGFR reporter. Transduction efficiency was evaluated through tEGFR expression four days following retroviral transduction. hCAR19 and tEGFR Treg each had ~30% tEGFR expression prior to enrichment (Figure 1D). Tregs were positively selected for tEGFR expression using MACS column purification to yield >85% EGFR+ Tregs with increased tEGFR

mean fluorescent intensity (MFI) (Figure 1C-D). MFI of CD25 and Foxp3 was comparable between non-transduced (NT), tEGFR control, and hCAR19 transduced Tregs (Figure E). The final Treg purity was ≥95% $CD25^{hi}Foxp3^{+}$ prior to experimental use (Figure 1F; Supplementary Figure 2).

***hCAR19 Treg stimulated through their CAR have increased expression of canonical Treg antigens and demonstrate enhanced metabolic fitness*.** Following stimulation with plate-bound recombinant hCD19 Fc protein for 48 hours, hCAR19 Treg relative to tEGFR Tregs had enhanced expression of canonical Treg antigens associated with suppression, including CTLA-4, TIGIT, Neuropilin 1 (Nrp1) and LAG-3 (Supplementary Figure 3A-D). Also, the proliferation marker Ki67, the activation marker CD71, and the lineage defining transcription factor Foxp3 were all expressed at higher levels on hCAR19 Tregs (Supplementary Figure 3E-G). These data suggested that hCAR19 compared to tEGFR Tregs may respond more robustly in vivo in hCD19 hemizygous recipients ($hCD19TG^{Tg/0}$), resulting in augmented immunosuppression and therapeutic protection.

In CAR19 human Tcons, utilizing a 4-1BB intracellular costimulatory domain as compared to CD28 significantly enhances respiratory capacity, fatty acid oxidation and mitochondrial biogenesis, all of which favors CD8 T-cell memory cells (37). In studies with CAR19 human Tregs, the same comparison showed a decrease in transcription of glycolysis genes (38). To determine whether CAR engagement could lead to differential metabolic states, hCAR19 and tEGFR murine Treg were stimulated on a hCD19 Fc coated plate for 48 hours prior to analysis. hCAR19 murine Treg had significantly increased expression of carnitine palmitoyl transferase I (CPT1a), the rate limiting enzyme for fatty acid oxidation (FAO), and the glucose transporter 1 (Glut1), as compared to tEGFR Treg (Supplementary figure 4A-B). Seahorse mitochondrial and glycolytic stress tests were performed to further explore the involvement of oxidative

phosphorylation and glycolysis by hCAR19 murine Tregs. hCAR19 Tregs had increased basal and maximal respiration, as well as spare respiratory capacity compared to tEGFR Treg (Supplementary Figure 4C-D), along with a significant increase in glycolysis, glycolytic capacity and glycolytic reserve (Supplementary Figure 4E-F). Together, these data show hCAR19 murine Treg stimulation by its cognate antigen results in increased energetic capacity, as evidenced by higher oxidative phosphorylation and glycolysis to support immunosuppressive functions.

***hCAR19 Tregs deplete hCD19 B cells and prevent systemic toxicity*.** To assess whether hCAR19 murine Tregs would induce B-cell aplasia, we utilized our previously published syngeneic mouse model in which hCD19TG$^{Tg/0}$ recipients are treated with cyclophosphamide (Cy) prior to CAR T-cell infusion. In this model, once hCAR19 murine CTLs are infused, recipients develop B-cell aplasia associated with systemic toxicity and a high degree of lethality by day 10 post-infusion (36). hCD19TG$^{Tg/0}$ recipients infused with hCAR19 murine Tregs or hCAR19 murine CD8 CTLs had 0.03% and 0.29% hCD19 B-cells on day 5 after adoptive cell transfer (ACT), respectively, whereas hCD19TG$^{Tg/0}$ recipients treated with Cy only had 17.7% splenic B-cells (Figure 2A-B). In contrast, tEGFR murine Treg and tEGFR murine CD8 CTL treated hCD19TG$^{Tg/0}$ mice had 13.9% and 13.0% hCD19 splenic B-cells. On day 10 after ACT, hCAR19 CD8 CTL treated hCD19TG$^{Tg/0}$ mice had 80% lethality compared to 0% lethality in the hCAR19 Treg group ($P< 0.05$, survival; Figure 2C). Additionally, hCD19TG$^{Tg/0}$ recipients of hCAR19 CD8 CTLs had 30% mean body weight loss compared to less than 10% in mice that received hCAR19 murine Tregs or either tEGFR subsets ($P<0.05$, day 5, Figure 2D). Furthermore, hCAR19 murine CD8 CTLs treated hCD19TG$^{Tg/0}$ mice had mean clinical scores that peaked at 5 on day 6 after ACT, while hCAR19 Treg, tEGFR CD8 CTL or tEGFR Treg treated hCD19TG$^{Tg/0}$ mice had consistently lower clinical scores of ≤2 , comparable to Cy only treated mice in the 8 days post-ACT (Figure 2E). These results demonstrate that hCAR19

murine Tregs cause B-cell aplasia without significant systemic toxicity or lethality in hCD19TG$^{Tg/0}$ recipients, in contrast to the severe side-effects and lethality of hCAR19 murine CD8 CTLs.

We also evaluated whether hCAR19 or tEGFR Treg could suppress the systemic toxicity induced by hCAR19 CD8 CTLs. Using a 2:1 ratio of hCAR19 CD8 CTL to hCAR19 or tEGFR Treg, we found that Treg treatment fully abrogated lethality in this model and significantly reduced clinical scores and weight loss (Supplementary Figure 5). hCAR19 Treg treated mice compared to tEGFR Treg demonstrated significantly higher mean weights that were maintained throughout the observation period, although there was no difference in clinical scores between these two cohorts, both of which were lower than hCAR19 CD8 CTLs (Supplementary Figure 5B-C). These data suggest hCAR19 Treg can be co-infused with hCD19 CD8 CTLs to reduce systemic toxicities.

hCAR19 Tregs control hCD19 TBL12^{luc} growth in vivo. To evaluate whether hCAR19 murine Tregs had the capacity to eliminate hCD19 TBL12^{luc} tumor cells in vivo, hCD19TG$^{Tg/0}$ mice were lethally irradiated, transplanted with 5x10^6 C57BL/6 T-cell depleted (TCD) bone marrow (BM). Cohorts were injected with 10^4 hCD19 TBL12^{luc} alone or no cells, and either hCAR19 Tregs, hCAR19 CD8 CTLs, tEGFR Tregs, or tEGFR CD8 CTLs. hCD19TG$^{Tg/0}$ recipients treated with either tEGFR Tregs or tEGFR CD8 CTLs had 100% lethality by day 18 and day 24, respectively, significantly faster than those receiving hCAR19 Tregs that required 28 days for uniform lethality. The best survival rate was observed in hCD19TG$^{Tg/0}$ mice treated with hCAR19 CD8 CTLs that had an 83.3% lethality rate by week 7 (Figure 3A), significantly better than all other cohorts receiving immune cell therapy.

On day 7 after transplantation, hCD19TG$^{Tg/0}$ mice injected with hCD19 TBL12^{luc} cells and tEGFR Tregs or tEGFR CD8 CTLs had detectable tumor by bioluminescent imaging (BLI). By day 14, only mice receiving hCD19 CD8 CTLs had no detectable tumor (Figure 3B-C). Notably, hCAR19 Treg and tEGFR CD8 CTL treated mice had significant tumor growth on day 14 and 20, ultimately leading to death in these mice before day 30 (Figure 3A-B). tEGFR Treg treated mice had a comparable mortality curve and tumor growth pattern to mice injected with hCD19 TBL12^{luc} only where mice began to have measurable tumor growth as early as day 7 after transplant and all succumbed to disease prior to day 20 (Figure 3A-C). hCAR19 CD8 CTLs largely controlled tumor growth during the first three weeks but ultimately had tumor outgrowth that led to 17% survival (Figure 3A-C). Overall, these data demonstrate hCAR19 Tregs can control hCD19 TBL12^{luc} growth in hCD19TG$^{Tg/0}$ mice early after a syngeneic transplant.

***hCAR19 Treg kill hCD19 TBL12^{luc} tumor cells in a perforin dependent, granzyme B independent manner*.** To better understand the mechanistic underpinnings of hCAR19 Treg mediated elimination of both hCD19+ B-cells and hCD19 TBL12^{luc} growth in vivo, we pursued phenotypic and functional analyses related to their cytolytic potential. Following stimulation of hCAR19 Tregs in a hCD19 Fc coated plated, we found that hCAR19 Tregs compared to tEGFR Tregs had a significant increase in the frequency and MFI of granzyme A (GzA), granzyme B (GzB), perforin (perf), and CD107α (Figure 4A-F; Supplementary Figure 6A-D). We next tested the killing potential of hCAR19 and tEGFR Treg by serial measurements over 48 hours using the IncuCyte Immune Cell Killing Assay. Tregs were co-cultured in the presence of either TBL12 or hCD19 TBL12^{luc} cells labeled with Far Red Dye and the IncuCyte Caspase 3/7 green apoptosis dye. We found hCAR19 Treg engaged in antigen-specific killing with only 7% live hCD19 TBL12^{luc} cells remaining after 48 hours of co-culture compared to 78% live TBL12 cells (Figure 4G). In contrast, wells containing tEGFR Treg had 87% live hCD19 TBL12^{luc} and 82% live TBL12 (Figure 4G).

We then assessed the expression of cytolytic molecules following anti-CD3/CD28 Dynabead stimulation used for retroviral transduction. hCAR19 and tEGFR CD8 CTLs expressed comparable levels of GzA and GzB, whereas hCAR19 and tEGFR Tregs had negligible expression (Supplementary Figure 6E). While Fas was increased in Treg compared with CTL, perforin, FasL and CD107α were comparably expressed (Supplementary Figure 6E). Next, to evaluate the killing potential of hCAR19 Treg compared to hCAR19 CTL, a flow cytometry killing assay was performed using Far Red labeled hCD19 TBL12^{luc} cells at a 5:1 effector to target (E:T) ratio. hCAR19 and tEGFR Tregs were sorted after retroviral transduction to achieve the highest Treg purity and ensure killing was not associated with contaminating hCAR19 CD4 CTLs. After a 48 co-culture, tEGFR CD8 CTLs had 67% live hCD19 TBL12^{luc} cells, while tEGFR CD4 CTLs and tEGFRs Treg had 74% and 76%, respectively (Figure 4H; Supplementary Figure 6F). hCAR19 CD4 CTLs engaged in killing of hCD19 TBL12^{luc} with 56% live cells at 5:1 E:T and 33.3% at the 10:1 E:T ratio (Figure 4H). In contrast, hCAR19 Tregs and hCAR19 CD8 CTLs had 4% and 8% live hCD19 TBL12^{luc}, respectively (Figure 4H; Supplementary Figure 6F). Over multiple in vitro flow killing assays using a 5:1 E:T ratio, hCAR19 Tregs averaged 1-19% live hCD19 TBL12^{luc} cells which was not significantly different than hCAR19 CD8 CTL which had 1-13% live hCD19 TBL12^{luc} cells (data not shown).

To assess the role of cytolytic pathways in hCAR19 Treg mediated killing, concanamycin A (CMA) and Z-AAD-CMK inhibitors were used to inhibit the expression of perf and GzB, respectively. hCAR19 Treg killed hCD19 TBL12^{luc} in a perf-dependent, GzB-independent manner (Figure 4I, Supplementary Figure 7). After 48 hour co-culture, hCAR19 Treg resulted in 38% live hCD19 TBL12^{luc} which was essentially unchanged to 27% live hCD19 TBL12^{luc} when Z-AAD-CMK, a GzB inhibitor, was added. In marked contrast, hCAR19 Treg co-culture with a perf inhibitor resulted in 112% live hCD19 TBL12^{luc} (Figure 4I). Findings were similar with tEGFR Treg that showed no significant difference when co-cultured with a GzB inhibitor and

background, non-specific killing was abrogated when co-cultured with a perf inhibitor (Figure 4I, Supplementary Figure 7). Moreover, hCAR19 Treg derived from perf knockout mice (perf KO) had a ~2.5 fold reduction in hCD19 TBL12^{luc} killing (Figure 4J). To investigate whether hCAR19 Tregs could engage in non-specific killing of nearby Tcons in the presence of hCD19 B-cells, hCAR19 and tEGFR Treg were co-cultured with Tcons in the presence of WT or hCD19 TG$^{Tg/0}$ APCs. After 72 hours, hCAR19 and tEGFR Tregs had comparable viability of CD4 and CD8 Tcons in the presence of WT or hCD19 TG$^{Tg/0}$ APCs (Supplementary Figure 8). These data show hCD19 CAR Tregs kill in antigen dependent, perforin dependent and GzB independent manner.

hCAR19 Treg ameliorate acute GVHD onset and severity without toxicity. To ensure antigen would be present to activate hCAR19 Tregs early after allo-HSCT, we quantified hCD19 B-cells in hCD19TG$^{Tg/0}$ recipient mice after lethal irradiation and transplantation with BALB/c BM. Splenic and mesenteric lymph node (mLN) hCD19 B-cell frequencies decreased by 19% and 9% on day 1 after transplantation, whereas by day 7 splenic and mLN B-cell frequencies were decreased by 86% and 58%, respectively (Supplementary Figure 9). There was a further reduction by day 14 such that both spleen and mLN had ≥86% fewer cells compared to non-transplanted hCD19TG$^{Tg/0}$ mice (Supplementary Figure 9). Additionally, peripheral blood hCD19 B-cells decreased rapidly by ~75% on day 1 and had negligible detection by day 14 (Supplementary Figure 9). These data demonstrated hCD19 B-cells are present in the spleen and mLNs of hCD19TG$^{Tg/0}$ mice through day 7 and up to day 14 in the mLNs, providing antigen necessary for hCAR19 Tregs to be activated and engage in immunosuppressive functions.

We next asked if hCAR19 Tregs conferred higher aGVHD protection as compared to hCD19 CAR T-cells, as the addition of T-cells could accelerate aGVHD lethality due to its T-cell mediated pathogenesis (3). To investigate this question, hCD19TG$^{Tg/0}$ mice were lethally

irradiated a day prior to receiving BALB/c BM only, BM with Tcons to induce aGVHD, or BM with Tcons and either hCAR19 Tregs, hCAR19 CD4 CTLs, or hCAR19 CD8 CTLs on day 0 of allo-HSCT. hCAR19 Tregs significantly suppressed aGVHD as shown by the absence of lethality and with clinical scores and weights overlapping with that of the BM only group (Figure 5A-E). In contrast, hCAR19 CD4 CTLs significantly exacerbated disease, causing faster mortality compared to aGVHD only group (Figure 5A). hCAR19 CD4 and CD8 CTLs treated mice showed increased weight loss and clinical scores similar to that of the aGVHD group (Figure 5B-E). While aGVHD mice fully succumbed to disease by day 45 after transplant, aGVHD mice treated with hCAR19 CD8 CTLs or hCAR19 CD4 CTL died by day 55 and day 40, respectively (Figure 5A).

Next, we evaluated the contribution of hCD19 B-cells to hCAR19 Treg suppressive function. We co-cultured NT, tEGFR, and hCAR19 Tregs at multiple E:T ratios with CD25 depleted Tcons labeled with CTV dye to track their proliferation. Tregs and Tcons were isolated from BALB/c mice, whereas APCs were isolated from C57BL/6 background mice in order to mimic the allo-setting in our in vivo GVHD model. We found that hCAR19 Treg had significantly higher suppressive function at the 1:24 and 1:48 E:T ratios when co-cultured with hCD19 B-cell containing APCs as compared to WT APCs (Figure 6A). There were no significant differences in suppression amongst NT and tEGFR Tregs co-cultured with WT or hCD19 B-cell containing APCs, and hCAR19 Tregs with WT APCs (Figure 6A).

We then tested whether hCAR19 Tregs were dependent on hCD19 B-cell expression to enhance aGVHD suppression. hCD19TG$^{Tg/0}$ mice were lethally irradiated one day prior to receiving BALB/c BM only, BM with Tcons to induce aGVHD, or BM with Tcons and either hCAR19 or tEGFR Tregs ($1.25x10^6$) on day 0 of allo-HSCT. An additional cohort consisted of WT C57BL/6 recipient mice to evaluate hCAR19 Treg efficacy in the absence of hCD19 antigen.

To assess the differences between hCAR19 and tEGFR Tregs we infused suboptimal GVHD prophylaxis Treg doses at a 1:2 E:T ratio. hCAR19 Tregs significantly improved aGVHD survival compared to tEGFR Tregs (Figure 6B) with an overall survival of 57% vs 0% on day 120 after transplant. hCAR19 Tregs infused into WT mice resulted in only 20% survival suggesting a role of hCD19 B-cells in supporting hCAR19 Treg suppression of aGVHD. These data suggest hCD19 antigen is necessary for hCAR19 Treg enhanced function when compared to tEGFR Treg (Figure 6B). Consistent with survival data, hCD19TG$^{Tg/0}$ recipients treated with hCAR19 Tregs had significantly reduced clinical scores (Figure 6C-D) and maintained body weights comparable to that of BM only recipients (Figure 6E-F). hCD19TG$^{Tg/0}$ mice given tEGFR Tregs and WT mice given hCAR19 Tregs did not improve mean body weights over that of the aGVHD group (Figure 6E-F). Altogether, hCAR19 Tregs compared to tEGFR Tregs significantly reduced the onset and severity of aGVHD in hCD19 B-cell dependent manner.

hCAR19 Treg have greater expansion early after allo-HSCT and demonstrate enhanced suppression of colonic Tcons compared to tEGFR Tregs. To evaluate how hCAR19 Tregs reduce aGVHD lethality, we first quantified Treg expansion in vivo using bioluminescent imaging (BLI) of luciferase expressing Tregs. hCD19TG$^{Tg/0}$ mice treated with hCAR19 Tregs compared to tEGFR Tregs showed significantly improved BLI signal by day 5 after allo-HSCT (Figure 7A-B). Radiance in the tEGFR Treg group slowly increased over time and equalized to that of hCAR19 Treg by day 14 and remained comparable until the end of the observation period which was day 28 (Figure 7B). Results of BLI were confirmed by enumerating splenic Tregs. A higher frequency of CD25^{+}Foxp3^{+} Treg were observed in hCD19TG$^{Tg/0}$mice treated with hCAR19 Tregs compared to tEGFR Tregs on day 5 after allo-HSCT (Figure 7C). Additionally, hCAR19 Tregs compared to tEGFR Tregs caused a greater reduction in the frequency of day 5 splenic CD4 and CD8 Tcons, while both Treg groups comparably decreased the frequency of CD11c expressing monocytes and DCs (Supplementary Figure 10).

Next, we evaluated hCAR19 Treg homing and protection of the gastrointestinal tract (GIT), as the GIT is the target organ associated with the highest aGVHD morbidity and mortality (3). Both hCAR19 and tEGFR Tregs homed to the colon by day 14 after allo-HSCT (Figure 7D). hCAR19 Tregs significantly increased the Treg:CD4 and Treg:CD8 T-cell ratios (Figure 7E-F). These results correlated with the finding that hCAR19 Tregs more potently reduced the number of proinflammatory, TNFα and IFNγ-producing, colonic CD4 and CD8 T-cells (Figure 7G-J). These data suggest that hCAR19 compared to tEGFR Tregs have enhanced Treg expansion early after allo-HSCT leading to increased Treg:Tcon ratios and decreased numbers of Tcons in the colon, a key aGVHD target organ.

***hCAR19 Treg maintain graft-versus-tumor responses in the allo-HSCT setting*.** Increased aGVHD suppression and reduction of proinflammatory cytokine producing Tcons by hCAR19 Tregs could interfere with the graft-versus-tumor (GVT) response. Therefore, we evaluated whether hCAR19 Tregs had the capacity to deplete hCD19 B-cells in hCD19 $TG^{Tg/0}$ recipient mice in the allo-HSCT setting. Mice transplanted with BM, Tcons and hCAR19 Tregs had significantly lower frequencies and absolute numbers of hCD19 B-cells as compared to those receiving tEGFR Tregs or no Tregs (Figure 8A-C). To determine whether hCAR19 Tregs would interfere with the GVT response, $hCD19TG^{Tg/0}$ recipients were co-infused with hCD19 $TBL12^{luc}$ cells on day 0. $hCD19TG^{Tg/0}$ mice that received BM and hCD19 $TBL12^{luc}$ cells had 100% mortality related to lymphoma by day 20 (Figure 8D). In contrast, mice receiving BM with hCD19 $TBL12^{luc}$ and Tcons had 37.5% death by day 50 related to lymphoma with late deaths that occurred by day 80 related to aGVHD (Figure 8D). Mice treated with tEGFR Tregs had 75% death related to lymphoma by day 40, with the remainder fully succumbing to aGVHD by day 80 (Figure 8D). In striking contrast, mice treated with BM, Tcons, hCD19 $TBL12^{luc}$ cells and hCAR19 Treg had 100% survival (Figure 8D). In support of the survival data, mice injected with

hCD19 TBL12^{luc} in the absence of Tcons had measurable tumor growth on day 7, and significant expansion by day 14 providing evidence that the early deaths in this group were lymphoma related (Figure 8E). All mice except one treated with hCD19 TBL12^{luc} and Tcons demonstrated tumor growth control up to day 28, whereas the addition of tEGFR Treg led to measurable tumor growth starting on day 7 after allo-HSCT (Figure 8E-F), whereas hCAR19 Tregs potently suppressed tumor growth throughout the entirety of this study (Figure 8E-F). These data demonstrate hCAR19 Tregs, unlike tEGFR Tregs, not only potently suppressed aGVHD but maintained GVT by potentiating anti-tumor responses.

Discussion

Here, we utilized a syngeneic mouse model to demonstrate that hCAR19 Tregs depleted hCD19TG$^{Tg/0}$ recipient hCD19 B-cells without inducing systemic toxicities, as is seen with hCAR19 CD8 CTLs. In this same model, hCAR19 Tregs controlled hCD19 TBL12^{luc} tumor growth in vivo leading to a significant improvement in survival as compared to mice injected with tumor cells alone or tumor cells with tEGFR Tregs. In vitro killing assays demonstrated hCAR19 Tregs utilized the perforin pathway to mediate antigen-specific killing. In a fully MHC mismatched allo-HSCT murine model, hCAR19 Tregs suppressed aGVHD whereas hCAR19 CD8 CTLs failed to provide therapeutic protection. The presence of hCD19 B-cells in recipient mice was necessary for the enhanced suppressive function of hCAR19 Tregs compared to control tEGFR Tregs in our aGVHD model. We showed that hCD19TG$^{TG/0}$ mice treated with hCAR19 Treg had hCD19 B-cell depletion as early as day 5 after allo-HSCT; nonetheless there was significant Treg expansion on day 5 after allo-HSCT in hCAR19 Treg compared to tEGFR Treg treated hCD19$^{TG/0}$ mice with significantly improved suppression of pro-inflammatory producing T cells in the gut. Our findings are consistent with what is known in the literature which is that in order to have effective GVHD suppression it must occur early after allo-HSCT to

target the key GVHD induction stages, such as alloantigen priming (3). Importantly, the hCD19 B-cell killing capacity of hCAR19 Tregs provided an advantage to obtaining a GVT response directed against hCD19 TBL12^{luc}. These studies report for the first time a hCAR Treg therapy that suppresses aGVHD and kills antigen expressing tumor cells to prevent hCD19 lymphoma recurrence without causing systemic toxicities.

The efficacy of CAR T-cell therapy in treating B-cell malignances has been hindered by severe toxicities resulting from high levels of inflammatory cytokines (e.g., CRS) (32). While most CRS patients experience mild symptoms, some cases are severe or life threatening. A primary treatment for CRS is the IL-6Rα antagonist Tocilizumab (33). Corticosteroids are used for CRS resistant cases and for CAR-related neurological complications (32). Some reports indicate that corticosteroids can negatively affect CAR T-cell persistence and function (39, 40), while other reports do not link steroids to poorer outcomes (41). Nonetheless, CAR T-cell therapies that do not induce deleterious, systemic inflammation may prove more efficacious than existing ones.

Unlike CAR CD8 CTLs, CAR Tregs produced minimal inflammatory cytokines following antigen activation suggesting a low risk for CRS induction (31, 42). A direct comparison of CAR19 Treg to CAR19 CD8 CTL administration in a xenogeneic GVHD model showed that human CAR19 CD8 CTL treated mice had significant weight loss, increased clinical scores and elevated mouse IL-6 levels, in contrast to human CAR19 Tregs (43). In studies described here, we used a syngeneic mouse model of CAR T-cell toxicity (36) and found that mice treated with hCAR19 CD8 CTLs had significant weight loss, increased clinical scores, and 80% mortality, whereas hCAR19 Treg treated mice had minimal weight loss, low clinical scores and no mortality. Furthermore, we found that hCAR19 Tregs could be infused on the same day as hCAR19 CD8 CTL to significantly reduce clinical scores, weights, and abrogate lethality. These results align with the function of Tregs to maintain immune homeostasis and dampen excessive, deleterious

immune responses (44). These data are relevant as CAR Treg therapies move into the clinic with HLA-A2 CAR Tregs for mismatched kidney transplant recipients (NCT04817774).

Tregs use cytolysis as one mechanism to modulate immune responses (26, 45, 46), as well as non-cytolytic mechanisms of suppression (22-24). It remains unclear what signals drive Tregs to utilize killing pathways versus other mechanisms of suppression. CAR Tregs have demonstrated minimal killing of antigen positive cells (17, 43). However, *Boroughs et al* (2019) reported CAR19 human Tregs could kill CD19 expressing cells in vitro via the perforin GzB pathway (31). Our results align with *Boroughs et al* (2019), as we found hCAR19 Treg could also kill hCD19 TBL12^{luc} cells in vitro. We found hCAR19 Treg killed in an antigen dependent and GzB independent, perforin dependent manner. We extend these findings to report that hCAR19 Tregs reduce hCD19 TBL12^{luc} lymphoma cell growth in vivo and enhance survival when compared to mice treated with tumor cells alone or with tEGFR Treg. In contrast, *Imura et al* (2020) did not find significant killing in vitro by CAR19 human Treg albeit their CAR also included the CD28 costimulatory domain as the *Boroughs et al* (2019) study. Instead, they found CAR19 Treg suppressed B-cell differentiation, proliferation, and antibody production (43). Similar to our allogeneic model, they showed B-cells were not pathogenic or necessary for xenogeneic GVHD induction although hCD19 B-cell expression activated hCAR19 Tregs, thereby facilitating their expansion and immune suppressive functions (17, 38, 43). With differences in CAR Treg cytolytic potential amongst CAR Tregs, research is warranted to investigate what factors induce the cytolytic and concurrent immune suppressive functions in vivo. Nonetheless, cytolytic CAR Tregs may provide a novel therapeutic avenue that tackles key limitations of Treg cell therapy through suppression of GVHD while significantly reducing the risk for relapse in patients.

Although insufficient Treg purity could confound analysis of Treg cytolytic potential measured, some groups have sorted the top 2% of CD4^{+}CD25^{+} T-cells (22) or measured in vitro

suppressive function immediately prior to adding Tregs to killing assays (30). To address this concern, we sort purified transduced hCAR19 Treg from Foxp3-GFP$^+$ reporter mice to >95% Foxp3$^+$ cells to ensure high Treg purity. Supportive of the suppressive and cytolytic capacity of CAR19 CD4 Tregs, Roncarolo and colleagues enforced IL-10 expression in human CD4 T-cells to generate a Type 1 regulatory (Tr1)-like cell that was suppressive and yet acquired cytotoxic activity restricted to myeloid cells, including myeloid malignancies. These human Tr1-like cells suppressed xenogeneic GVHD and potentiated GVT responses (47). Therefore, it is possible that genetic modifications can generate an immune regulatory and suppressive cell capable of engaging in cytotoxicity towards a specific cell type.

We chose to evaluate the efficacy of Tregs redirected towards hCD19 on B-cells with an already FDA approved construct to facilitate translating our findings to the clinic. The hCAR19 construct used here contains the 4-1BB costimulatory domain associated with activated, effector Tregs (48) and enhanced oxidative phosphorylation, a preferred Treg metabolic program (37). However, recent studies of hCAR19 human Treg studies comparing CD28 and 4-1BB costimulatory domains have found 4-1BB based CAR Tregs had decreased suppressive function in vitro and in vivo (31, 38), although it can be rescued with transient mTOR inhibition (49). Rapamycin mediated mTOR inhibition was utilized in our hCAR19 Treg cultures in an effort to maintain Treg purity (50). Interestingly, a study reported that 4-1BB agonist treatment induced a subset of CD4$^+$Foxp3$^+$ Treg to eliminate virus induced tumor cells in mice (51) and the addition of 4-1BB expression in CAR T-cells with an intracellular CD28 costimulatory domain improved their proliferation and cytotoxicity (52). The exact role 4-1BB signaling plays in Treg cytolytic potential has not been fully elucidated.

Relapse of the original hematological malignancy following allo-HSCT remains a major challenge and the leading cause of allo-HSCT failure resulting in a dismal prognosis (53). Treatment of relapse with salvage chemotherapy, donor lymphocyte infusions (DLI), and second

transplants have low success rates (54). Thus, treatment strategies that reduce the risk of relapse and improve treatment outcomes are necessary. Prophylactic DLI have shown a significant decrease in relapse rates for patients with myeloid leukemias but comes at the cost of increased incidence of GVHD (55). Here we show that hCAR19 Tregs given with Tcons suppress aGVHD and tumor growth throughout the duration of our transplants, in stark contrast to mice treated with Tcons alone and Tcons with tEGFR Tregs. This suggest that using cytolytic CAR Tregs specific for antigens of the patient's hematologic condition might significantly reduce both GVHD and relapse. CAR Treg infusion in combination with post-transplant cyclophosphamide could be particularly effective in preventing GVHD, as the mechanism of post-transplant cyclophosphamide action appears to depend on Treg (56). A combination of CAR Treg infusion, post-transplant cyclophosphamide and further GVHD prophylaxis with a Treg-supportive drug such as sirolimus (rapamycin) could be a potent anti-GVHD regimen without compromising GVT. Furthermore, cytolytic CAR Tregs may have sufficient anti-tumor response to be co-infused with DLI to suppress GVHD while maintaining anti-tumor effects, or given alone to exploit their dual suppressive and cytolytic properties. Further, cytolytic CAR Tregs offer the possibility of expanding the clinical applications of CAR Treg therapy to autoimmunity, chronic inflammation, and transplantation. CAR Tregs allow targeting of cells responsible for the pathophysiology of certain diseases while simultaneously enhancing Treg expansion and suppression of ongoing inflammatory disease.

There are some limitations in our hCD19Tg$^{Tg/0}$ model that must be considered before reaching extrapolation of hCAR19 Treg efficacy in patients. hCD19Tg$^{Tg/0}$ mice which express the hCD19 transgene on B-cells have significantly lower B-cell frequencies compared to WT mice and elevated B-cell hCD19 density when compared to human B-cells (36). While these attributes in B-cells represent differences found in our mouse model from that in humans, the aggregate effects of high hCD19 density with a relative B-cell hypoplasia created a CRS induced lethality

model upon infusion of hCAR19 CD8 T cells. CRS has been reported immune deficient mice carrying a high burden of hCD19 lymphoma cells (57), whereas CRS was only observed in syngeneic, immune competent hCD19Tg$^{Tg/0}$ mice that have high hCD19 density coupled with less B cell hypoplasia than hCD19Tg$^{Tg/Tg}$ mice (36, 58). Thus, it is possible that the elevated hCD19 density might cause hCAR19 CD8T cell hyper-responsiveness leading to CRS. Whether hyper-responsiveness is necessary to activate hCAR19 Tregs in our model is not clear. Similarly unclear is the dependency of hCAR19 CD8 CTL persistence on a critical B-cell mass or hCD19 density, although in general B-cell aplasia has been ascribed to be a surrogate for persistent CAR19 CD8 CTLs. Future studies may consider boosting hCD19 engagement by periodic infusions of hCD19-Fc protein. Regardless of the mechanistic underpinnings of the CRS, we have demonstrated a novel mechanism by which hCAR19 Tregs can be activated in vivo to suppress GVHD and maintain GVL responses without the risk of CRS.

In summary, to our knowledge, this is the first report that a CAR Treg therapy can control tumor growth in vivo with the capacity to suppress GVHD without CAR associated toxicities. These findings expand our understanding of CAR Treg function and inform future Treg therapy design and application. The novel approach of redirecting CAR Treg to tumor antigens is a therapeutic avenue with the potential to improve outcomes in allo-HSCT patients by reducing the risk of GVHD and relapse.

Methods

Mice. BALB/c, C57BL/6, and CD45.1 female mice were purchased from Charles River Laboratory. C57BL/6-Prf1 KO mice were purchased from Jackson Laboratory. Dr. Thomas Tedder kindly provided hCD19TG$^{Tg/Tg}$ mice. We bred hCD19TG$^{Tg/Tg}$ mice with C57BL/6 mice to generate hCD19TG$^{Tg/0}$. We also bred hCD19TG$^{Tg/Tg}$ mice with BALB/c mice to generate hCD19$^{Tg/0}$ CB6F1. B6 Foxp3-GFP knock in (KI) mice were kindly provided by Vijay Kuchroo and bred in our animal colony. B6 Foxp3-GFP-Luciferase mice were bred in our animal colony. All mice were housed in a specific pathogen-free facility and used with University of Minnesota Institutional Animal Care and Use Committee approval.

Cell culture. Tregs and T-cells were cultured in Expansion Media, a DMEM based media (DMEM, high glucose, pyruvate; Thermo Fisher) supplemented with 10% fetal bovine serum (Premium; Atlanta biologicals), 10mM HEPES (Sigma-Aldrich), 1x NEAA (Fisher Scientific), 1x Penicillin /Streptomycin (Sigma-Aldrich), 50ug/mL Gentamicin (Gentamicin sulfate, liquid, Corning®), 55mM 2-mercaptoethanol (Sigma-Aldrich). TBL12 and hCD19 TBL12^{luc} cell lines were cultured in RPMI-1640 (Thermo Fisher) supplemented with 10% fetal bovine serum (FBS) (Thermo Fisher), 10 mM HEPES (Sigma-Aldrich), 1x Penicillin /Streptomycin (Sigma-Aldrich), 1x NEAA (Fischer Scientific), and 55mM 2-mercaptoethanol (Sigma-Aldrich).

Isolation of primary murine Tcons and Tregs. CD4 and CD8 T-cells (Tcons) were purified from spleens by negative selection using biotin-labeled anti-CD19 (1D3), B220 (RA3-6B2), CD11b (M1/70), CD11c (N418), NK1.1 (PK136), CD49b (DX5) CD25 (PC61.5), γδ, (GL3) and TER-119 (TER-119), followed by streptavidin RapidSphere depletion with EasySep magnet (StemCell Technologies). Tregs were purified from lymph node and spleen using negative selection as above but with the addition of anti-CD8 (53-6.7) and in the absence of anti-CD25 to enrich for CD4$^+$CD25$^+$ T-cells. CD4$^+$CD25$^+$ T-cells were then incubated with PE-labeled anti-CD25

antibody (PC61.5, eBioscience), followed by anti-PE beads (Miltenyi Biotec), and $CD25^+$ cells were selected via magnetic columns (Miltenyi Biotec). Treg from wildtype mice were stained with anti-CD4 (Biolegend; GK1.5), anti-CD25 (Thermofisher; PC61.5), and Fixable viability dye eFluor 780 (eBioscience) to be sorted as $CD4^+CD25^{hi}$ cells. Treg from Foxp3-GFP mice were sorted as $CD25^{hi}GFP^+$ from $CD4^+$ T-cells using a BD LSR II/Fortessa/Canto.

Plasmid construction and retroviral transduction. The hCAR19 construct was subcloned from a lentivirus into a MT71 retroviral vector which was optimized for T-cell expression. Tregs were activated with anti-CD3/CD28 Dynabeads (Thermofisher) at a 3:1 bead to Treg ratio in Expansion Media with 2000 IU/mL of recombinant human IL-2 (Proleukin) and 5 nM rapamycin (Sigma Aldrich). On day 3 after Treg harvest, a 48 well plate was coated with RetroNectin (Takara), retrovirus containing the tEGFR or hCAR19-tEGFR construct was added and spinoculated for 2 hours at 2000 rpm. Supernatant was discarded and $1x10^6$ Tregs were added per well and spinoculated for 15 mins at 1500 rpm. After spinoculation, Treg were incubated at 37 C, 5% CO_2 with a media change every 48 hours. Tcon were activated with anti-CD3/CD28 Dynabeads (Thermofisher) at a 1:1 Tcon:bead ratio in Expansion Media with 100 IU/mL of recombinant human IL-2 (Proleukin). On day 2 after Tcon harvest, a 24 well plate was coated with retronectin (Takara), retrovirus containing the tEGFR or hCAR19-tEGFR construct was added and spinoculated for 2 hours at 2000 rpm. Supernatant was discarded and $0.5x10^6$ Tcons were added per well and spinoculated for 15 mins at 1500 rpm. After spinoculation, Tcons were incubated at 37 C, 5% CO_2 with a media change every 48 hours. On day 8 after harvest, we measured transduction efficiency via tEGFR expression. To enrich for tEGFR+ transduced cells, Tregs or Tcons were stained with anti-human EGFR (AY13) and then incubated with anti-PE beads (Miltenyi Biotec) to be selected via magnetic column.

aGVHD and GVT model: hCD19TG$^{Tg/0}$ recipients were lethally irradiated with 11 Gy a day prior to transplantation, and then injected IV with 5x10^6 BALB/c BM, BM with 2.5x10^6 CD25^{neg} BALB/c Tcon, or BM with Tcon and 1.25x10^6 hCAR19 Treg or CTL, tEGFR Treg or CTL. Mice were evaluated for daily survival, weights, and evidence of clinical GVHD as previously described (59). hCD19 TBL12^{luc} is a B-cell lymphoma cell line of B6 origin (60) that has been modified to express human CD19 antigen on B-cells, as well as express luciferase. hCD19TG$^{Tg/0}$ were lethally irradiated with 11 Gy a day prior to transplantation. hCD19TG$^{Tg/0}$ were injected IV with 5x10^6 TCD BM from BALB/c mice alone or injected with TCD BM plus 2.5x10^6 CD25^{neg} Tcons and 10^4 hCD19 TBL12^{luc}, or TCD BM with Tcons and hCD19 TBL12^{luc} and 1.25x10^6 of either hCAR19 or tEGFR Tregs. Tumor growth was monitored by luciferase imaging of lymphoma cells. To directly measure Treg anti-tumor responses in vivo, we used a similar experimental design except we set up a syngeneic transplant where each group received 5x10^6 C57BL/6 TCD BM with 1.0x10^6 hCAR19 or tEGFR Tregs in the absence of Tcons.

Bioluminescent imaging (BLI) studies. We intraperitoneally injected firefly luciferin substrate (0.1 mL at 30 mg/ml, Promega) into recipient mice and waited 5 minutes prior to imaging. The Xenogen IVIS imaging system was used and data was analyzed using the Living Image 3.0 Software.

In vitro Treg suppression assay. T-cell depleted splenocytes and B cells were isolated from either wildtype C57BL/6 mice or hCD19TG$^{Tg/0}$ and mixed at 1:1 ratio to generate antigen presenting cells (APCs). CD25 depleted T-cells were isolated from BALB/c mice and stained with 2.5 uM Cell Trace Violet (Life Technologies) for 10 mins at 37C to track proliferation. Tregs were also isolated from BALB/c mice and transduced as described above. Anti-CD3 (0.25 ug/ml,145-2C11, eBioscience) was added to the assay to stimulate T-cell proliferation.

553 *Colon Lymphocyte Isolation*. We isolated the lamina propia lymphocytes using a protocol
554 previously described (61). Briefly, mice were sacrificed on day 14 after allo-HSCT, the colons
555 were harvested and flushed with PBS containing 10% FBS. Colon was cut into pieces and
556 washed twice for 10 mins at 37C with a cell dissociation buffer (Ca/Mg free PBS with 5 nM
557 EDTA and 10 nM HEPES). Tissues were washed once with PBS containing 10% FBS for 5
558 mins at 37C, and then cut into smaller pieces prior to being treated three times for 20 mins at
559 37C with a digestion buffer -1 mg/ml Collagenase D (Roche), 0.15 IU/ml Dispase (Worthington),
560 and 0.5 mg/mL DNaseI (Roche) in Ca/Mg free PBS containing 10% FBS. Lymphocyte were
561 purified using a 40% and 80% Percoll (Sigma) gradient.

562 *Cytotoxicity Assays.* For the IncuCyte killing assay, we used TBL12 or hCD19 TBL12^{luc} cells
563 which were labeled with CellTrace Far Red (Thermo Fisher Scientific) and incubated with either
564 hCAR19 or tEGFR Treg at a 2:1 E:T ratio for 48 hours. IncuCyte Caspase-3/7 green apoptosis
565 assay reagent (Essen Biosciences) was also added per well. Images were taken every few
566 minutes and the number of apoptotic cells per well was quantified using the IncuCyte Caspase-
567 3/7 green apoptosis assay reagent and the IncuCyte Zoom platform (Essen Biosciences). For
568 the flow cytometry killing assay, we used hCD19 TBL12^{luc} cells which were stained using the
569 CellTrace Far Red (Thermo Fisher Scientific) and incubated with either hCAR19 or tEGFR
570 Tregs, CD4 T-cells, or CD8 T-cells at a 5:1 E:T ratio for 48 hours. Killing was calculated through
571 viability measured using the Fixable Viability Dye of the Far Red stained tumor cells (62).

572 *In vivo toxicity measurement.* We used a previously published model where effectors are
573 adoptively transferred into hCD19TG$^{Tg/0}$ recipient mice a day after receiving lymphodepleting
574 dose of 300 mg/kg of Cytoxan (36). 3x10^6 effectors were injected IV to the tail vein. Survival,
575 weights and clinical scores were recorded daily. Scores are assigned a 0-2 on each of the four
576 criteria: activity, fur texture, posture, and weight. A score of 0 compared to 8 indicates a healthy
577 and moribund mouse, respectively (59).

Metabolic Flux Analysis. With XFe-96 Extracellular Flux Analyzer (Seahorse Bioscience) we measured oxygen consumption rates (OCR) and extracellular acidification rates (ECAR) using the XF media (modified DMEM containing 2.5mM glucose, 2mM glutamine, and 1mM sodium pyruvate). OCR was measured in response to 1μM oligomycin, 1μM fluorocarbonyl cyanide phenylhydrazone (FCCP), and 1μM antimycin, while ECAR was measured in response to 20mM Glucose, 1μM oligomycin and 80mM 2-deoxyglucose (2-DG). Prior to seahorse analysis Treg were stimulated in hCD19 Fc coated plate (R&D systems,0.02 ug/ul).

Flow cytometry. Fluorochrome-conjugated monoclonal/polyclonal antibodies were purchased from eBioscience, Abcam, and BD Bioscience. anti-mouse CD4 (GK1.5), anti-mouse CD25 (PC61.5, anti-mouse Foxp3 (FJK-16s), anti-mouse CD8 (53-6.7), anti-human CD19 (H1B19), anti-human EGFR (AY13) anti-mouse CD45.1 (A20), anti-mouse CTLA-4 (UC10-4B9), anti-mouse Neuropilin 1 (eDS304M), anti-mouse Lag 3 (C9B7W), anti-mouse CD11c (N418) anti-mouse IFNγ (XMG1.2), anti-mouse TNFα (MP6-XT22), anti-mouse Fas (SA367H8), anti-mouse FasL (MFL3), anti-mouse Perforin (eBioMAK-D), anti-mouse GzB (NGZB), anti-mouse GzA (3G8.5), anti-mouse CD107α (1D4B), anti-mouse CD71 (R17217), anti-mouse CPT1a (8F6AE9), anti-mouse Glut1 (ER3915), and Fixable viability dye eFluor 780. Intracellular staining was performed using the fixation/permeabilization concentrate (Cat# 5123-43) and diluent (Cat# 5223-56) buffer solutions and IC buffer (Cat# 8333-56), according to the eBioscience Foxp3 staining kit. Stained cells were analyzed on a LSR Fortessa Flow Cytometer (BD Biosciences) and data were analyzed using FlowJo software (Tree Star, Ashland, OR, USA).

Statistics. Data are presented as mean ± SD. Statistical analyses were performed using Student's unpaired *t* test with Bonferroni correction for multiple comparisons when necessary or a Log-rank (Mantel Cox) test in survival studies using GraphPad Prism version 9 software. *p* values less than 0.05 was considered statistically significant.

Study approval. Animals studies were conducted in accordance with a protocol reviewed and approved by the IACUC of the University of Minnesota (2103A38904).

Author contributions:

SBW designed and performed experiments, analyzed results, and wrote the manuscript. MLL designed and performed experiments, and analyzed results. SJ, CMH, JHL, MHT, EAA performed experiments, discussed results, and edited the manuscript. MCJ, JEW edited the manuscript. MJO generated retroviral constructs and edited the manuscript. GT, BHK, AS, CAP, and BRB contributed to experimental design, discussed results, and edited the manuscript.

Acknowledgements

This work was funded by the National Institute of Allergy and Infectious Diseases (NIAID), National Heart, Lung, and Blood Institute (NHLBI) and National Cancer Institute (NCI) under grant numbers NIH R01 56067, R37 AI34495, R01 HL11879, R01 HL155114; P01 CA 065493; T32 AI007313 and F30 HL156312; T32 HL007062. We would like to give special thanks to Peter Hinderlie for his help with the IncuCyte experiments.

References

1. Kernan NA, et al. Analysis of 462 transplantations from unrelated donors facilitated by the National Marrow Donor Program. *N Engl J Med.* 1993;328(9):593-602.
2. Holtan SG, et al. Composite end point of graft-versus-host disease-free, relapse-free survival after allogeneic hematopoietic cell transplantation. *Blood.* 2015;125(8):1333-8.
3. Zeiser R, and Blazar BR. Acute Graft-versus-Host Disease - Biologic Process, Prevention, and Therapy. *N Engl J Med.* 2017;377(22):2167-79.
4. Pidala J, and Anasetti C. Glucocorticoid-refractory acute graft-versus-host disease. *Biol Blood Marrow Transplant.* 2010;16(11):1504-18.
5. Wingard JR, et al. Long-term survival and late deaths after allogeneic hematopoietic cell transplantation. *J Clin Oncol.* 2011;29(16):2230-9.
6. Hill L, et al. New and emerging therapies for acute and chronic graft versus host disease. *Ther Adv Hematol.* 2018;9(1):21-46.
7. Welniak LA, et al. Immunobiology of allogeneic hematopoietic stem cell transplantation. *Annu Rev Immunol.* 2007;25:139-70.
8. Hill GR, et al. Current Concepts and Advances in Graft-Versus-Host Disease Immunology. *Annu Rev Immunol.* 2021;39(1):19-49.
9. Romano M, et al. Past, Present, and Future of Regulatory T Cell Therapy in Transplantation and Autoimmunity. *Front Immunol.* 2019;10(43).
10. Brunstein CG, et al. Infusion of ex vivo expanded T regulatory cells in adults transplanted with umbilical cord blood: safety profile and detection kinetics. *Blood.* 2011;117(3):1061-70.
11. Taylor PA, et al. The infusion of ex vivo activated and expanded CD4(+)CD25(+) immune regulatory cells inhibits graft-versus-host disease lethality. *Blood.* 2002;99(10):3493-9.
12. Brunstein CG, et al. Umbilical cord blood-derived T regulatory cells to prevent GVHD: kinetics, toxicity profile, and clinical effect. *Blood.* 2016;127(8):1044-51.
13. Hoffmann P, et al. Donor-type CD4(+)CD25(+) regulatory T cells suppress lethal acute graft-versus-host disease after allogeneic bone marrow transplantation. *J Exp Med.* 2002;196(3):389-99.
14. Cohen JL, et al. CD4(+)CD25(+) immunoregulatory T Cells: new therapeutics for graft-versus-host disease. *J Exp Med.* 2002;196(3):401-6.
15. Martelli MF, et al. HLA-haploidentical transplantation with regulatory and conventional T-cell adoptive immunotherapy prevents acute leukemia relapse. *Blood.* 2014;124(4):638-44.
16. Di Ianni M, et al. Tregs prevent GVHD and promote immune reconstitution in HLA-haploidentical transplantation. *Blood.* 2011;117(14):3921-8.
17. MacDonald KG, et al. Alloantigen-specific regulatory T cells generated with a chimeric antigen receptor. *J Clin Invest.* 2016;126(4):1413-24.
18. Maldini CR, et al. CAR T cells for infection, autoimmunity and allotransplantation. *Nat Rev Immunol.* 2018;18(10):605-16.
19. Ellis JM, et al. Frequencies of HLA-A2 alleles in five U.S. population groups: Predominance of A∗02011 and identification of HLA-A∗0231. *Hum Immunol.* 2000;61(3):334-40.
20. Kansal R, et al. Sustained B cell depletion by CD19-targeted CAR T cells is a highly effective treatment for murine lupus. *Sci Transl Med.* 2019;11(482).
21. Ellebrecht CT, et al. Reengineering chimeric antigen receptor T cells for targeted therapy of autoimmune disease. *Science.* 2016;353(6295):179-84.
22. Grossman WJ, et al. Human T regulatory cells can use the perforin pathway to cause autologous target cell death. *Immunity.* 2004;21(4):589-601.

23. Zhao DM, et al. Activated CD4+CD25+ T cells selectively kill B lymphocytes. *Blood.* 2006;107(10):3925-32.
24. Gondek DC, et al. Cutting edge: Contact-mediated suppression by CD4+CD25+ regulatory cells involves a granzyme B-dependent, perforin-independent mechanism. *J Immunol.* 2005;174(4):1783-6.
25. Gondek DC, et al. Transplantation survival is maintained by granzyme B+ regulatory cells and adaptive regulatory T cells. *J Immunol.* 2008;181(7):4752-60.
26. Bolivar-Wagers S, et al. Cytolytic CD4(+) and CD8(+) Regulatory T-Cells and Implications for Developing Immunotherapies to Combat Graft-Versus-Host Disease. *Front Immunol.* 2022;13:864748.
27. Wing J, and Sakaguchi S. Multiple treg suppressive modules and their adaptability. *Front Immunol.* 2012;3.
28. Sakaguchi S, et al. Regulatory T Cells and Human Disease. *Annu Rev Immunol.* 2020;38(1):541-66.
29. Plitas G, and Rudensky AY. Regulatory T Cells in Cancer. *Annu Rev Cancer Biol.* 2020;4(1):459-77.
30. Choi BD, et al. Human regulatory T cells kill tumor cells through granzyme-dependent cytotoxicity upon retargeting with a bispecific antibody. *Cancer Immunol Res.* 2013;1(3):163.
31. Boroughs AC, et al. Chimeric antigen receptor costimulation domains modulate human regulatory T cell function. *JCI insight.* 2019;5(8):e126194.
32. Brudno JN, and Kochenderfer JN. Toxicities of chimeric antigen receptor T cells: recognition and management. *Blood.* 2016;127(26):3321-30.
33. Siegler EL, and Kenderian SS. Neurotoxicity and Cytokine Release Syndrome After Chimeric Antigen Receptor T Cell Therapy: Insights Into Mechanisms and Novel Therapies. *Front Immunol.* 2020;11.
34. Schmidts A, et al. Toward Better Understanding and Management of CAR-T Cell–Associated Toxicity. *Annu Rev Med.* 2021;72(1):365-82.
35. Shimabukuro-Vornhagen A, et al. The role of B cells in the pathogenesis of graft-versus-host disease. *Blood.* 2009;114(24):4919-27.
36. Pennell CA, et al. Human CD19-Targeted Mouse T Cells Induce B Cell Aplasia and Toxicity in Human CD19 Transgenic Mice. *Mol Ther.* 2018;26(6):1423-34.
37. Kawalekar OU, et al. Distinct Signaling of Coreceptors Regulates Specific Metabolism Pathways and Impacts Memory Development in CAR T Cells. *Immunity.* 2016;44(2):380-90.
38. Dawson NAJ, et al. Functional effects of chimeric antigen receptor co-receptor signaling domains in human regulatory T cells. *Sci Transl Med.* 2020;12(557):eaaz3866.
39. Brentjens RJ, et al. CD19-targeted T cells rapidly induce molecular remissions in adults with chemotherapy-refractory acute lymphoblastic leukemia. *Sci Transl Med.* 2013;5(177):177ra38.
40. Davila ML, et al. Efficacy and toxicity management of 19-28z CAR T cell therapy in B cell acute lymphoblastic leukemia. *Sci Transl Med.* 2014;6(224):224ra25.
41. Sun Z, et al. The Association Between Glucocorticoid Administration and the Risk of Impaired Efficacy of Axicabtagene Ciloleucel Treatment: A Systematic Review. *Front Immunol.* 2021;12.
42. Koristka S, et al. Engrafting human regulatory T cells with a flexible modular chimeric antigen receptor technology. *J Autoimmun.* 2018;90:116-31.
43. Imura Y, et al. CD19-targeted CAR regulatory T cells suppress B cell pathology without GvHD. *JCI Insight.* 2020;5(14).
44. Sakaguchi S, et al. Regulatory T cells: how do they suppress immune responses? *Int Immunol.* 2009;21(10):1105-11.

45. Ren X, et al. Involvement of cellular death in TRAIL/DR5-dependent suppression induced by CD4+CD25+ regulatory T cells. *Cell Death Differ.* 2007;14(12):2076-84.
46. Cao X, et al. Granzyme B and Perforin Are Important for Regulatory T Cell-Mediated Suppression of Tumor Clearance. *Immunity.* 2007;27(4):635-46.
47. Locafaro G, et al. IL-10-Engineered Human CD4(+) Tr1 Cells Eliminate Myeloid Leukemia in an HLA Class I-Dependent Mechanism. *Mol Ther.* 2017;25(10):2254-69.
48. Bacher P, et al. Regulatory T Cell Specificity Directs Tolerance versus Allergy against Aeroantigens in Humans. *Cell.* 2016;167(4):1067-78.e16.
49. Lamarthée B, et al. Transient mTOR inhibition rescues 4-1BB CAR-Tregs from tonic signal-induced dysfunction. *Nat Commun.* 2021;12(1):6446.
50. Battaglia M, et al. Rapamycin selectively expands CD4+CD25+FoxP3+ regulatory T cells. *Blood.* 2005;105(12):4743-8.
51. Akhmetzyanova I, et al. CD137 Agonist Therapy Can Reprogram Regulatory T Cells into Cytotoxic CD4+ T Cells with Antitumor Activity. *J Immunol.* 2016;196(1):484-92.
52. Dai Q, et al. 4-1BB Signaling Boosts the Anti-Tumor Activity of CD28-Incorporated 2nd Generation Chimeric Antigen Receptor-Modified T Cells. *Front Immunol.* 2020;11.
53. Barrett AJ, and Battiwalla M. Relapse after allogeneic stem cell transplantation. *Expert Rev Hematol.* 2010;3(4):429-41.
54. Rager A, and Porter DL. Cellular therapy following allogeneic stem-cell transplantation. *Ther Adv Hematol.* 2011;2(6):409-28.
55. de Lima M, et al. Prophylactic donor lymphocyte infusions after moderately ablative chemotherapy and stem cell transplantation for hematological malignancies: high remission rate among poor prognosis patients at the expense of graft-versus-host disease. *Bone Marrow Transplant.* 2001;27(1):73-8.
56. Ganguly S, et al. Donor CD4+ Foxp3+ regulatory T cells are necessary for posttransplantation cyclophosphamide-mediated protection against GVHD in mice. *Blood.* 2014;124(13):2131-41.
57. Giavridis T, et al. CAR T cell-induced cytokine release syndrome is mediated by macrophages and abated by IL-1 blockade. *Nat Med.* 2018;24(6):731-8.
58. Davila ML, et al. CD19 CAR-targeted T cells induce long-term remission and B Cell Aplasia in an immunocompetent mouse model of B cell acute lymphoblastic leukemia. *PLoS One.* 2013;8(4):e61338.
59. Cooke KR, et al. An experimental model of idiopathic pneumonia syndrome after bone marrow transplantation: I. The roles of minor H antigens and endotoxin. *Blood.* 1996;88(8):3230-9.
60. Bjordahl RL, et al. iNKT cells suppress the CD8+ T cell response to a murine Burkitt's-like B cell lymphoma. *PLoS One.* 2012;7(8):e42635.
61. Saha A, et al. Programmed death ligand-1 expression on donor T cells drives graft-versus-host disease lethality. *J Clin Invest.* 2016;126(7):2642-60.
62. Nacasaki Silvestre R, et al. In: Swiech K, Malmegrim KCR, and Picanço-Castro V eds. *Chimeric Antigen Receptor T Cells: Development and Production*. New York, NY: Springer US; 2020:213-22.

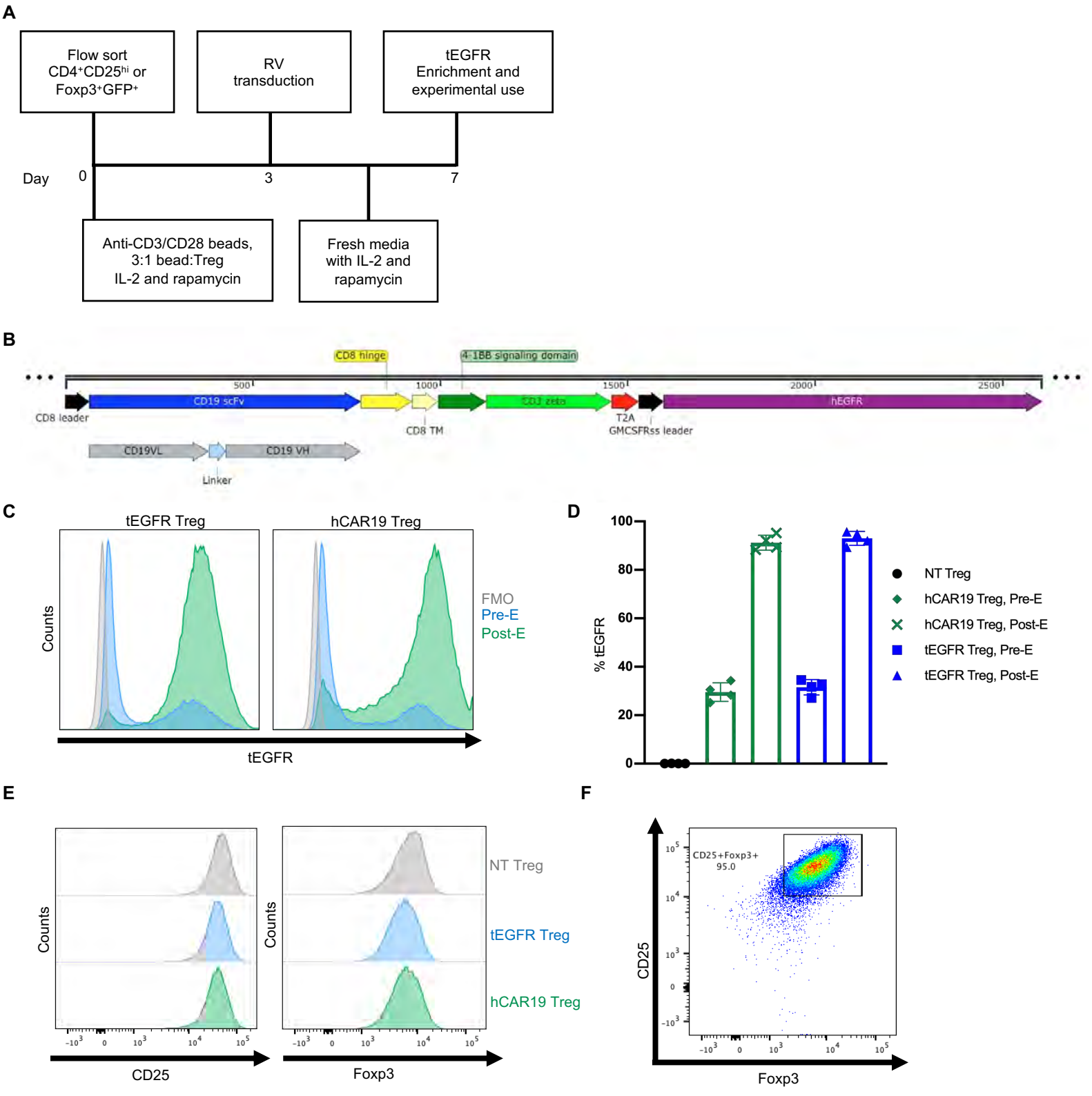

Figure 1. Generation of hCAR19 Treg. (**A**) Schema of hCAR19 and tEGFR Treg generation. (**B**) Schematic representation of hCAR19 construct in a pMP71 vector backbone. scFv, single chain variable fragment; VL, variable light chain; VH, variable heavy chain; TM, transmembrane domain. (**C**) Representative histogram plots of tEGFR expression in hCAR19 and tEGFR control transduced Treg prior to experimental use. FMO, fluorescence minus one; pre-E, before tEGFR positive enrichment; post-E, following tEGFR positive enrichment. (**D**) Percentage of tEGFR expression in non-transduced Treg (NT), pre and post tEGFR enrichment of hCAR19 and tEGFR transduced Treg. (**E**) Histogram plots of CD25 and Foxp3 expression in NT, tEGFR, and hCAR19 Treg. (**F**) Representative FACS plot of CD25^{+}Foxp3^{+} transduced hCAR19 Treg prior to experimental use.

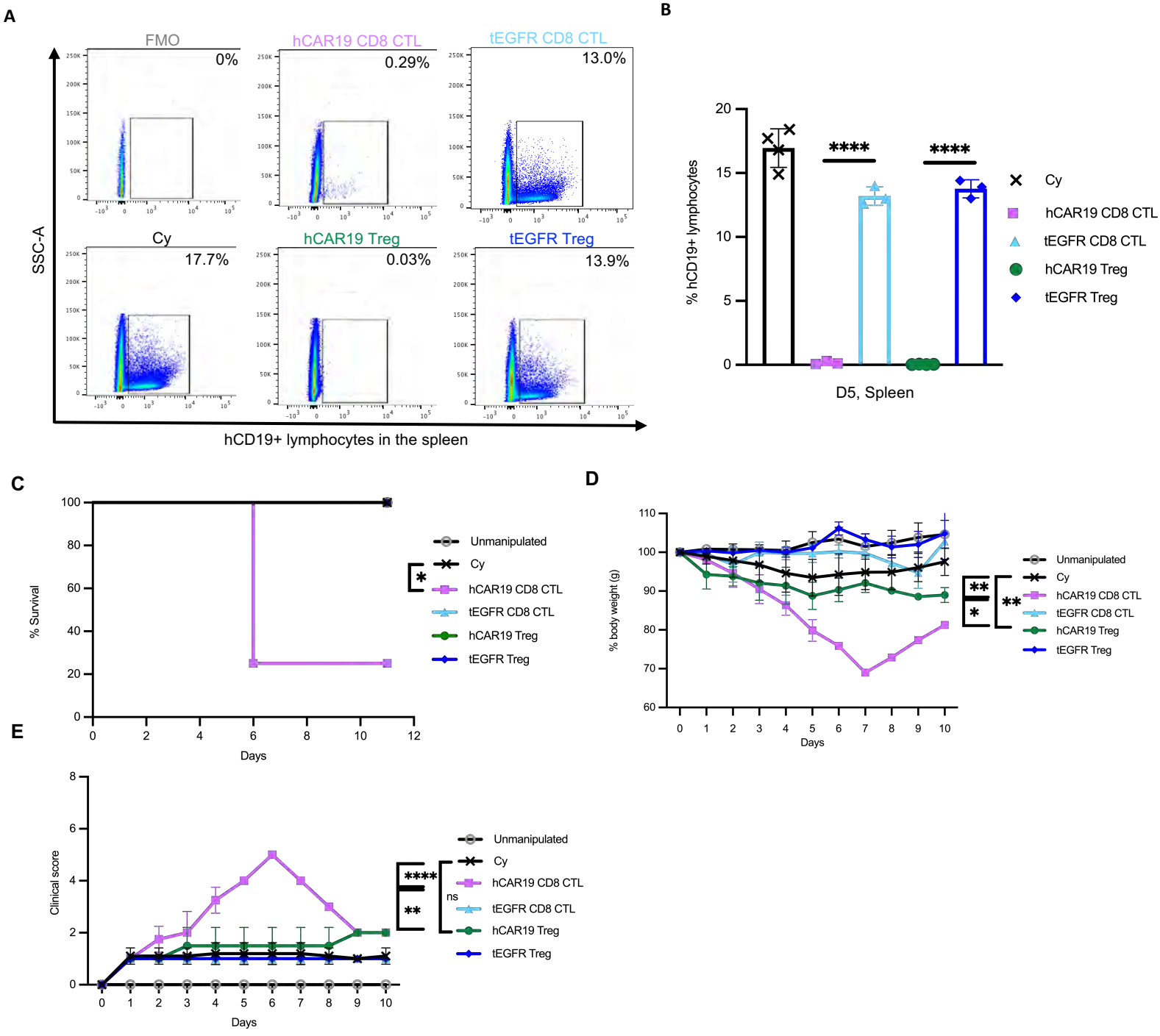

Figure 2. hCAR19 Treg deplete hCD19 B-cells and prevent systemic toxicities in a syngeneic mouse model. hCD19TG$^{Tg/0}$ recipient mice injected with 300 mg/kg of cyclophosphamide (Cy) a day prior to adoptive cell transfer (ACT) with C57BL/6 hCAR19 or tEGFR Tregs, or hCAR19 or tEGFR CD8 T-cells (CTL). (**A**) Representative flow cytometry plots and quantification (**B**) of hCD19+ lymphocytes in the spleen on day five after ACT. Cy, n=4; hCAR19 CD8 CTL, n=3**;** tEGFR CD8 CTL, n=3; hCAR19 Treg, n=4; tEGFR Treg, n=3. Data is representative from two independent experiments. (**C**) Survival. (**D**) Percent body weight. (**E**) Clinical scores. Unmanipulated, n=4; Cy, n=4; hCAR19 CD8 CTL, n=4**;** EGFR CD8 CTL, n=3; hCAR19 Treg, n=3; tEGFR Treg, n=3. Data is representative of three independent experiments. Statistics are shown on day five after ACT. Student t test with Bonferroni correction for multiple comparison was used for statistical analysis. Log rank test was used to analyze survival curves. Error bars indicate the standard deviation of the mean. ns: no significance; *:<0.5 ; **: <0.01; ***:<0.001; ****:<0.0001.

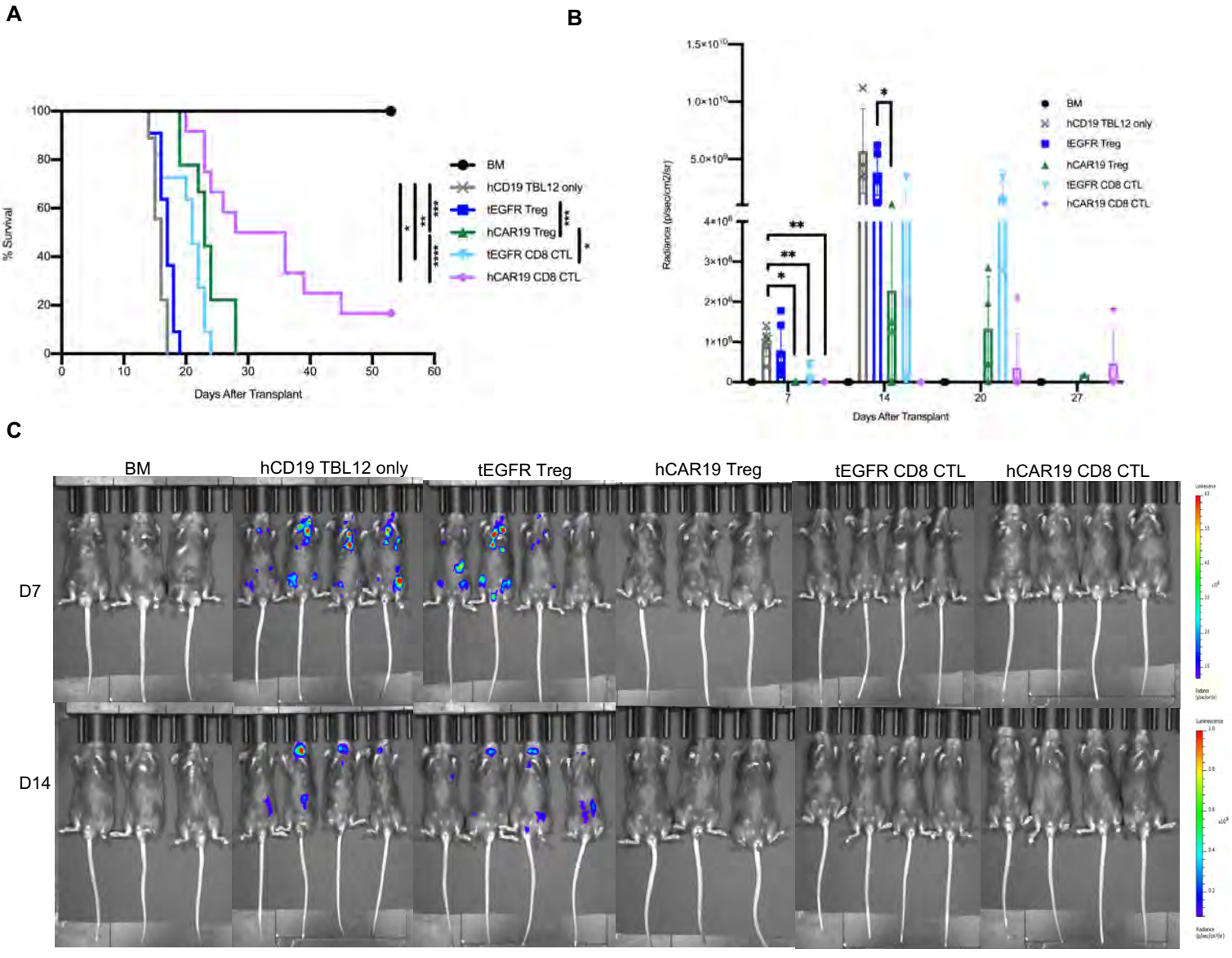

Figure 3. hCAR19 Treg have anti-tumor responses in the absence of Tcon in a syngeneic tumor model. Survival (**A**) and average radiance (**B**) of hCD19TG$^{TG/0}$ mice after undergoing a lethal irradiation prior to receiving C57BL/6 bone marrow (BM), BM with hCD19 TBL12^{luc} cells, or BM with hCD19 TBL12^{luc} cells and either tEGFR or hCAR19 Tregs or CTLs. CTLs in this experiment were CD8 T-cells. Survival: BM, n=10; hCD19 TBL12^{luc}, n=9; tEGFR Treg, n=11; hCAR19 Treg, n=9; tEGFR CTL, n=11; hCAR19 CTL, n=12. Data is pooled from two independent experiments. Average radiance: BM, n=6; hCD19 TBL12^{luc}, n=6; tEGFR Treg, n=7; hCAR19 Treg, n=6; tEGFR CTL, n=6; hCAR19 CTL, n=7. Only 3-4 mice were imaged per group. Data is pooled from two independent experiments. (**C**) Representative images of hCD19TG$^{TG/0}$ mice on day 7 and 14 after syngeneic HSCT. Student t test with Bonferroni correction for multiple comparison was used for statistical analysis. Log rank test was used to analyze survival curves. Error bars indicate the standard deviation of the mean. ns: no significance; *:<0.5 ; **: <0.01; ***:<0.001; ****:<0.0001.

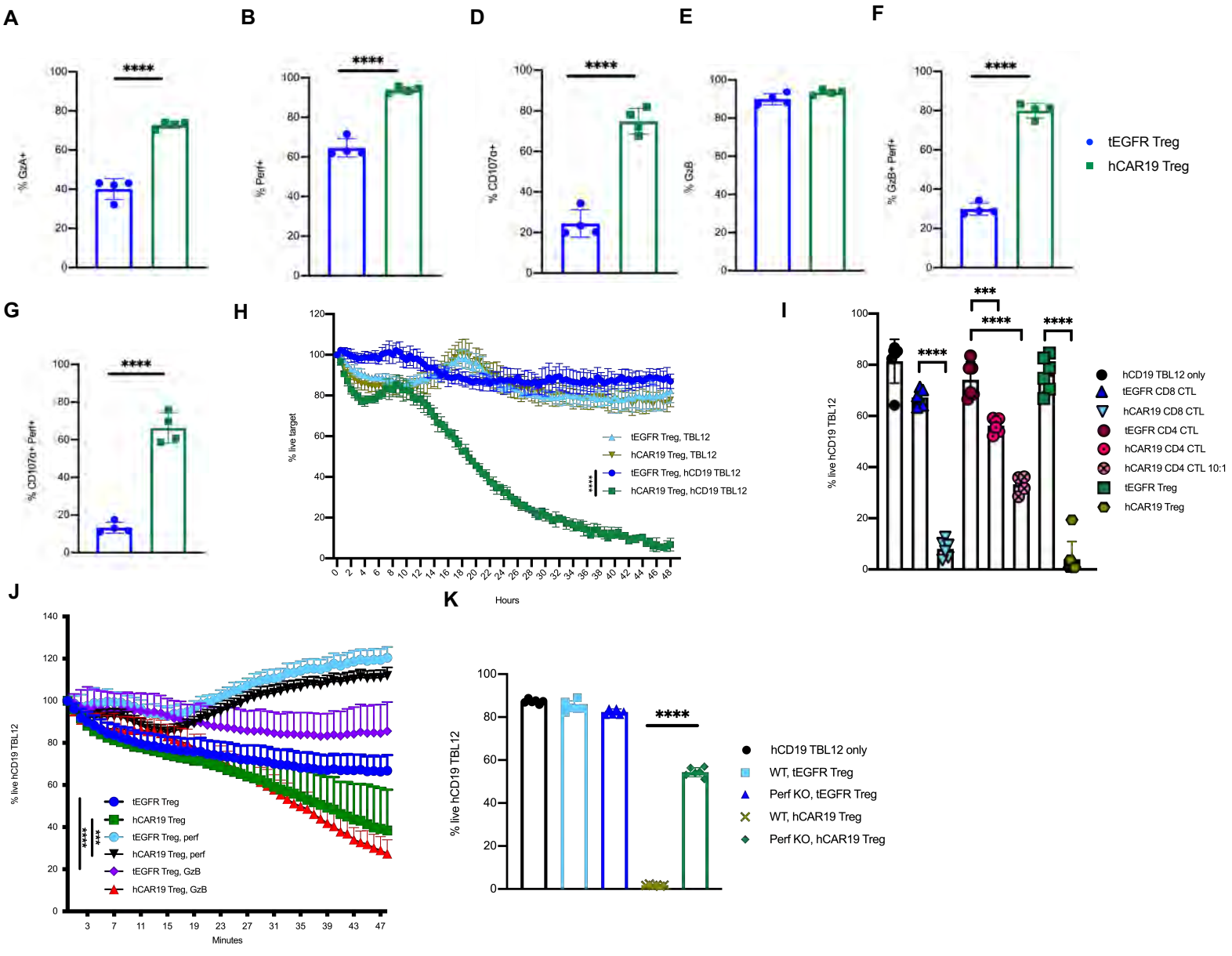

Figure 4. hCAR19 Treg have increased expression of killing markers after antigen specific activation and engage in *in vitro* killing of hCD19 TBL12. (**A**-**F**) Frequency of hCAR19 or tEGFR Treg expressing granzyme A (GzA), perforin (perf), CD107α, and granzyme B (GzB) after 48 hour stimulation in hCD19 Fc coated plate. hCAR19 Treg, n=4; tEGFR Treg, n=4. (**G**) IncuCyte in vitro killing assay with TBL12 and hCD19 TBL12^{luc} tumor cells stained with Far Red Dye and the IncuCyte Caspase 3/7 green apoptosis dye. E:T ratio used was 2:1. n=3 for all groups. (**H**) 48 hour flow cytometry in vitro killing assay using hCD19 TBL12^{luc} with sorted Foxp3^{+}GFP^{+} Treg the day of experiment using a 5:1 E:T ratio in all groups except when noted to be 10:1. n=6 for all groups. (**I**) IncuCyte in vitro killing assay using the perforin (per) inhibitor concanamycin A (CMA) and granzyme B (GzB) inhibitor Z-AAD-CMK with hCD19 TBL12^{luc} tumor. E:T ratio used was 2:1. n=5 for all groups, except for hCAR19 Treg and hCAR19 Treg GzB had n=3. (**J**) 48 hour flow cytometry in vitro killing assay using hCD19 TBL12^{luc} at an E:T ratio of 5:1. n=6 for all groups. Statistics for IncuCyte experiments were done at the 48 hour timepoint. Data in this figure is representative from two independent experiments. Student t test with Bonferroni correction for multiple comparisons was used for statistical analysis. Error bars indicate the standard deviation of the mean. ns: no significance; *:<0.5 ; **: <0.01; ***:<0.001; ****:<0.0001.

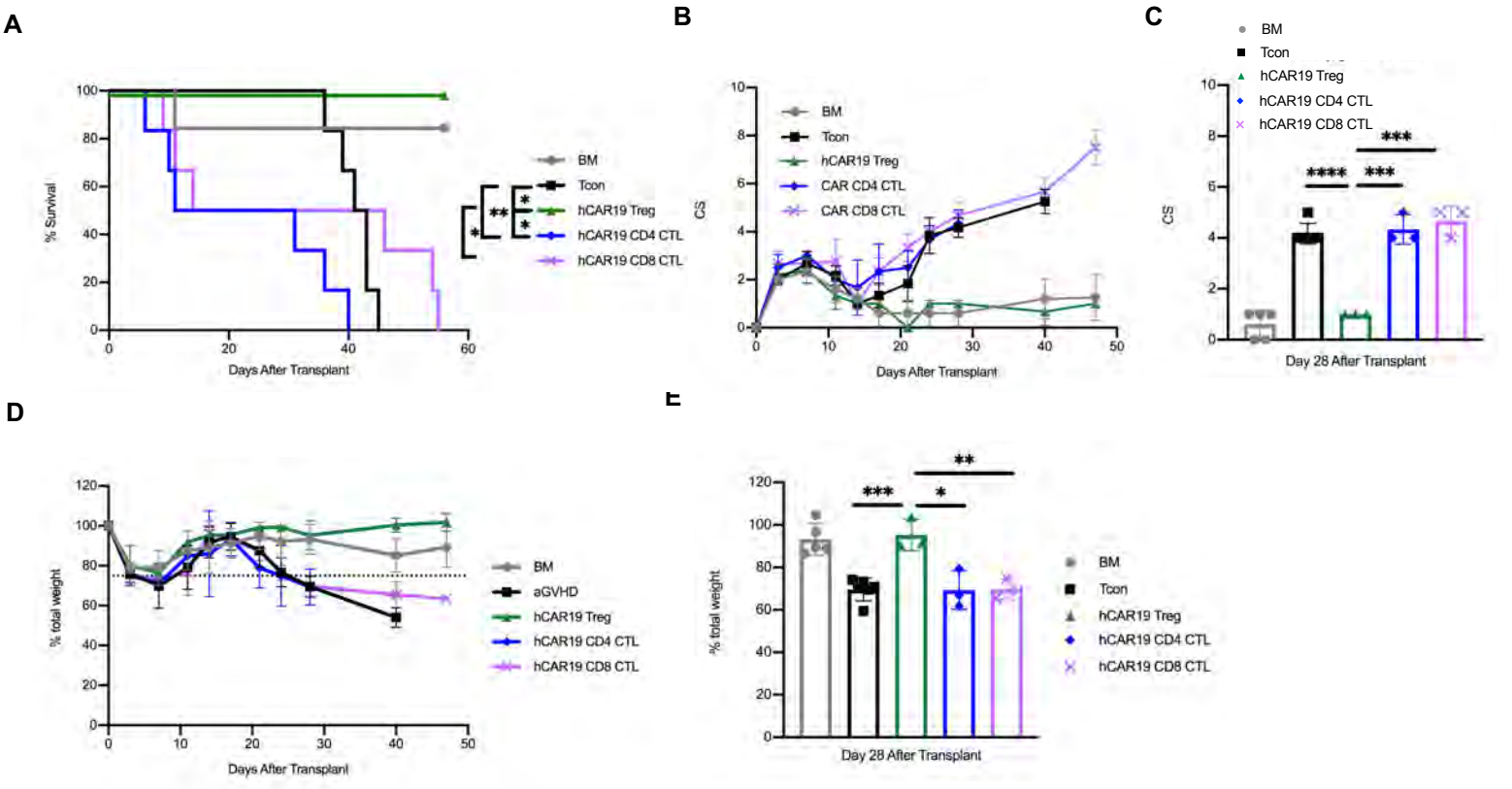

Figure 5. hCAR19 Treg reduce aGVHD severity and mortality relative to hCAR19 CTL. (**A**) Survival for hCD19TG$^{TG/0}$ recipient mice after undergoing a lethal irradiation prior to receiving BALB/c BM only, BM with Tcon (Tcon), or BM with Tcon and either hCAR19 Treg, hCAR19 CD4 CTL, or hCAR19 CD8 CTL. BM, n=6; Tcon, n=6; hCAR19 Treg, n=6; hCAR19 CD4 CTL, n=6; hCAR19 CD8 CTL, n=6. Data is representative from two independent experiments. (**B**) Clinical GVHD Scores; 0: no disease, 10: severe disease. (**C**) Clinical scores quantified on day 28. (**D**) Percent body weight. (**E**) Percent body weight quantified on day 28. Student t test with Bonferroni correction for multiple comparisons was used for statistical analysis. Log rank test was used to analyze survival curves. Error bars indicate the standard deviation of the mean. ns: no significance; *:<0.5 ; **: <0.01; ***:<0.001; ****:<0.0001.

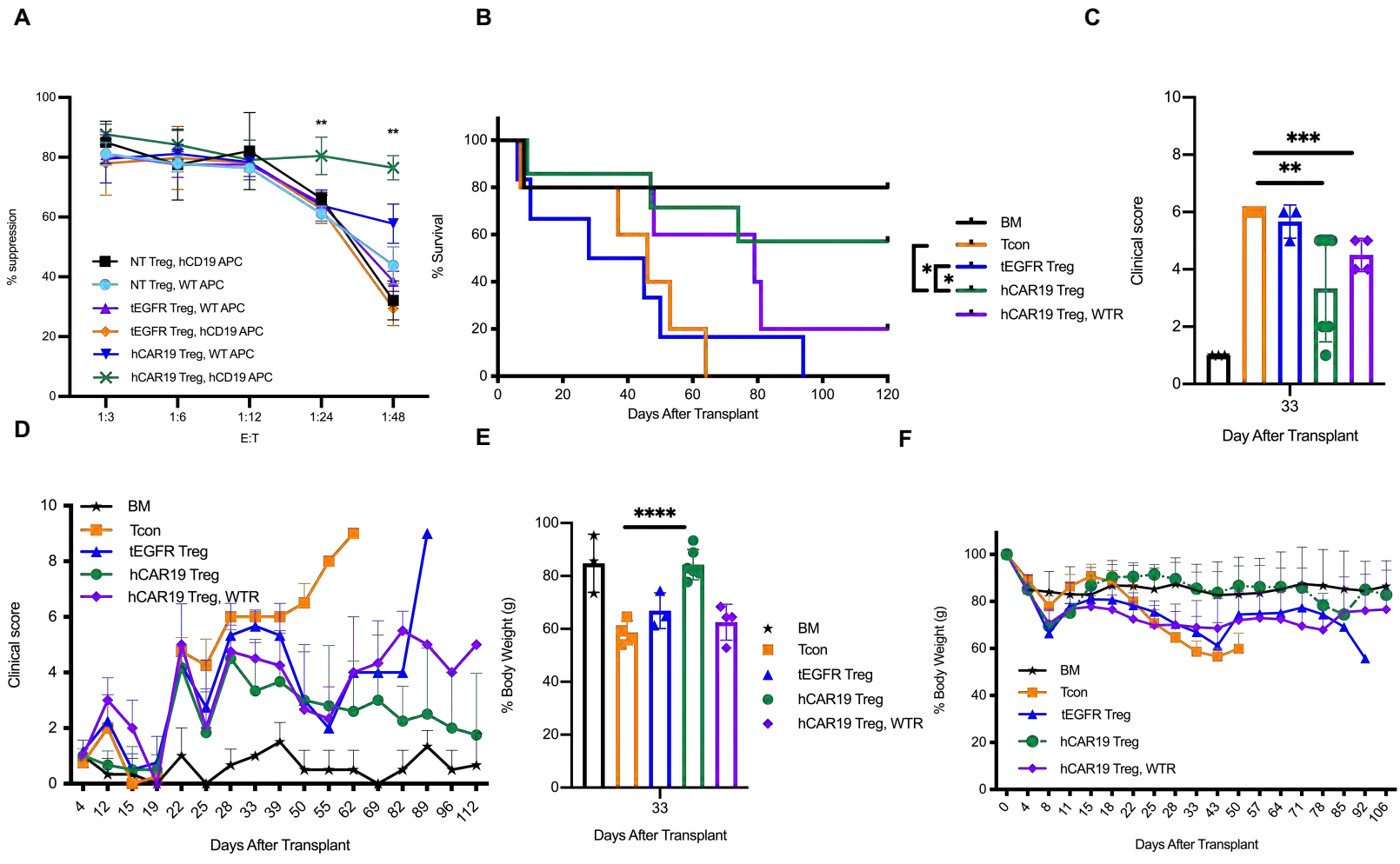

Figure 6. hCAR19 Treg reduce aGVHD severity and improve overall survival in a hCD19 dependent manner. (**A**) Percent suppression by NT, tEGFR, or hCAR19 Treg of CD8 T-cells in the presence of wildtype (WT) or hCD19 containing B cells. NT, non-transduced; APC, antigen presenting cells; E:T, effector to target ratio. (**B**) Survival for hCD19TG$^{TG/0}$ recipient mice after undergoing a lethal irradiation prior to receiving 5x10^6 BALB/c BM, BM with 2.5x10^6 Tcon (Tcon), or BM with Tcon and either 1.25x10^6 hCAR19 or tEGFR Treg; or WT C57BL/6 recipient mice receiving BALB/c BM with Tcon and hCAR19 Treg (hCAR19 Treg, WTR). BM, n=5; Tcon, n=8; tEGFR Treg, n=6; hCAR19 Treg, n=6; hCAR19 Treg WTR, n=5. Data is representative from four independent experiments. (**C-D**) Clinical GVHD Scores; 0: no disease, 10: severe disease. (**C**) Clinical GVHD scores quantified on day 33. (**E**) Percent body weight quantified on day 33. (**F**) Percent body weight. Student t test with Bonferroni correction for multiple comparisons was used for statistical analysis of weights and clinical scores. Log rank test was used to analyze survival curves. Error bars indicate the standard deviation of the mean. ns: no significance; *:<0.5 ; **: <0.01; ***:<0.001; ****:<0.0001.

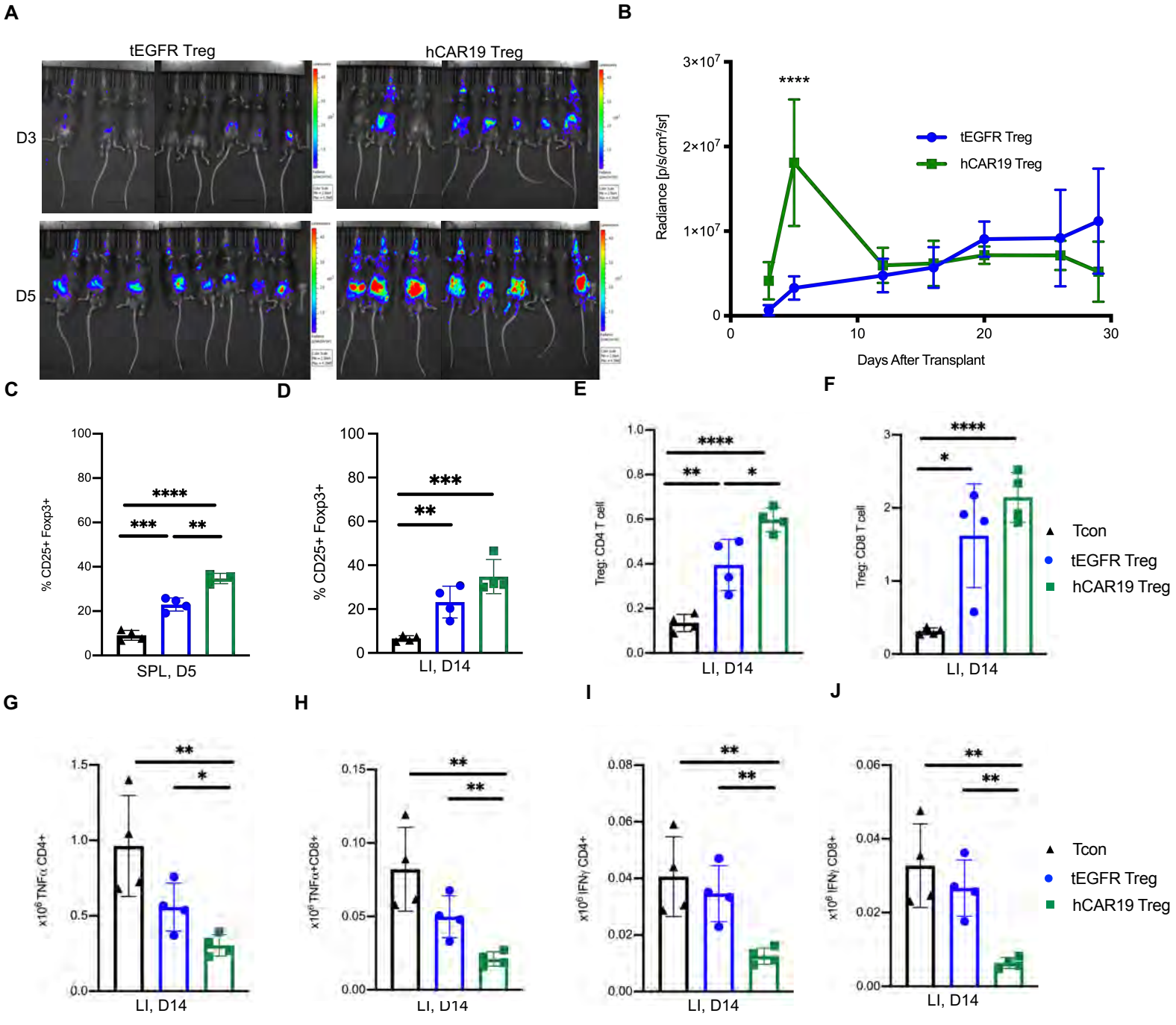

Figure 7. hCAR19 Treg have increased expansion and suppression of activated T-cells in the colon following allo-HSCT. (**A**) Images of hCD19TG$^{TG/0}$ mice on day 3 and 5 after receiving BALB/c bone marrow (BM) with Tcon and luciferase+ hCAR19 or tEGFR Treg. (**B**) Average radiance of luciferase+ hCAR19 or tEGFR Tregs from day 3 to 30 after allo-HSCT. tEGFR Treg, n=8; hCAR19 Treg, n=8. (**C**) Frequency of CD25^{+}Foxp3^{+} Tregs in the spleen on day 5 after allo-HSCT. Tcon, n=4; tEGFR Treg, n=4; hCAR19 Treg, n=3. (**D-J**) Colon was harvested on day 14 after allo-HSCT in hCD19TG$^{TG/0}$ recipient mice that received BALB/c BM with Tcon (Tcon), or BM with Tcon and tEGFR or hCAR19 Treg. (**E-F**) Treg to CD4 and CD8 T-cell ratio. (**G-J**) Absolute number of TNFα+ and IFNγ+ CD4 and CD8 T-cells. Tcon, n=4; tEGFR Treg, n=4; hCAR19 Treg, n=4. Data from all experiments is representative from two independent experiments. Student t test with Bonferroni correction for multiple comparison was used for statistical analysis. Error bars indicate the standard deviation of the mean. ns: no significance; *:<0.5 ; **: <0.01; ***:<0.001; ****:<0.0001.

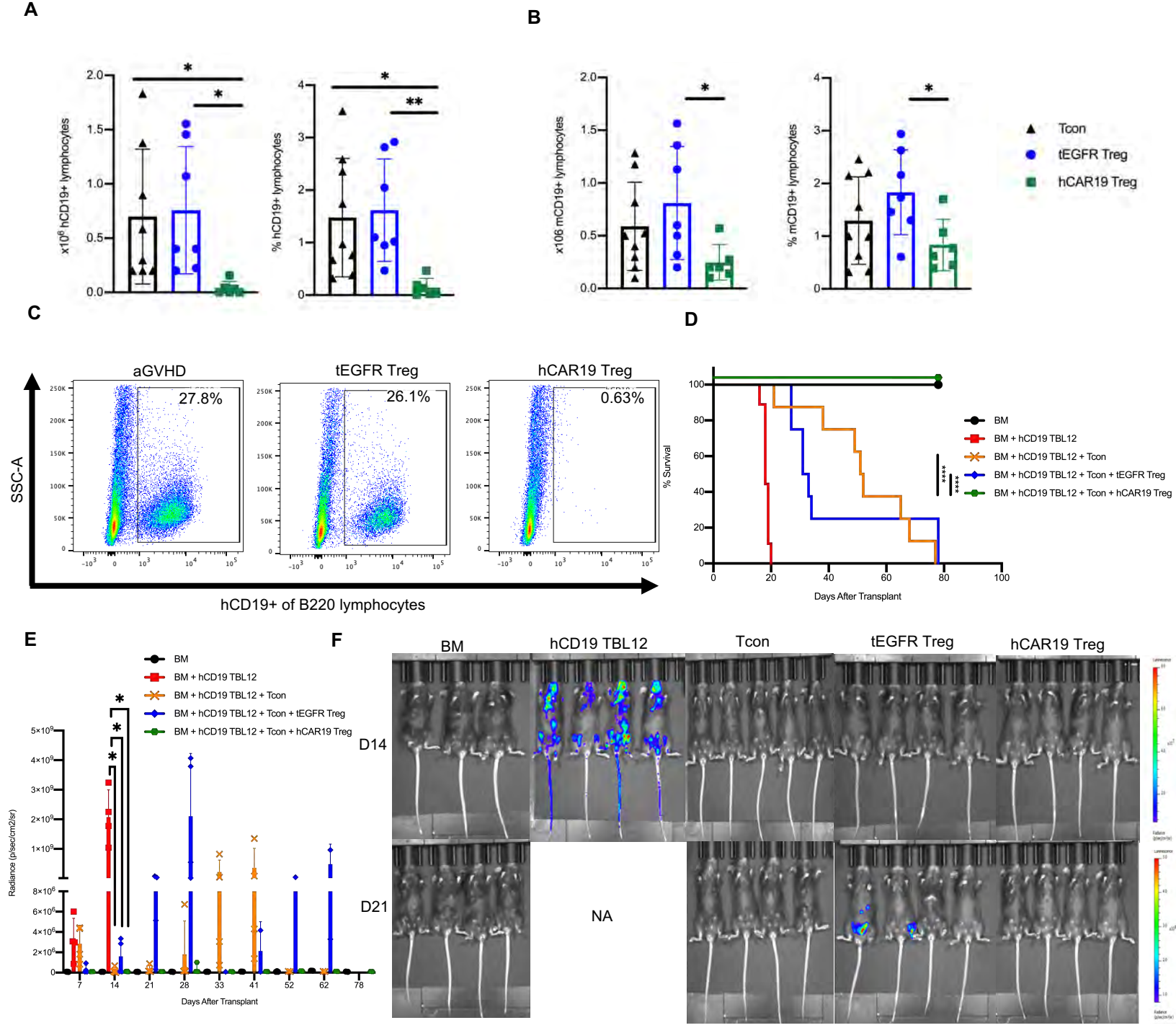

Figure 8. hCAR19 Treg maintain graft versus tumor responses. (**A**) Absolute number and frequency of hCD19+ and mCD19+ (**B**) lymphocytes in the spleen on day 5 of hCD19TG$^{TG/0}$ recipient mice after undergoing a lethal irradiation prior to receiving BALB/c bone marrow (BM) with Tcon (Tcon), or BM with Tcon and either hCAR19 or tEGFR Treg. Data is pooled from two independent experiments. Tcon, n=8; tEGFR Treg, n=7; hCAR19 Treg, n=6. (**C**) Representative flow plots demonstrating hCD19+ lymphocyte depletion in hCAR19 Treg treated mice on day 5 after allo-HSCT. hCD19 lymphocytes were gated from live B220 cells. (**D**) Survival of hCD19TG$^{TG/0}$ recipient mice after undergoing a lethal irradiation prior to receiving BALB/c BM, BM with hCD19 TBL12, BM with hCD19 TBL12 with Tcon (Tcon), or BM with hCD19 TBL12 and Tcon and either hCAR19 or tEGFR Treg. Data is representative from two independent experiments. BM, n=7; hCD19 TBL12^{luc}, n=9; Tcon, n=8; tEGFR Treg, n=8; hCAR19 Treg, n=9. (**E**) Average radiance of hCD19 TBL12^{luc}. Average radiance: BM, n=4; hCD19 TBL12^{luc}, n=4; tEGFR Treg, n=4; hCAR19 Treg, n=4. Only 3-5 mice were imaged per group. Data is representative from two independent experiments. (**F**) Images from day 14 and 21 after allo-HSCT. Student t test with Bonferroni correction for multiple comparisons was used for statistical analysis. Log rank test was used to analyze survival curves. Error bars indicate the standard deviation of the mean. ns: no significance; *:<0.5 ; **: <0.01; ***:<0.001; ****:<0.0001.